

Assessment of ion exchange resins as catalysts for the direct transformation of fructose into butyl levulinate

Eliana Ramírez, Roger Bringué, Carles Fité, Montserrat Iborra, Javier Tejero^(*), Fidel Cunill

Department of Chemical Engineering and Analytical Chemistry, Faculty of Chemistry, University of Barcelona, Martí i Franquès 1, 08028- Barcelona, Spain

Abstract

The transformation of fructose into butyl levulinate in aqueous 1-butanol (initial molar ratio 1-butanol/fructose 79, and butanol/water 1.19) has been studied in a discontinuous reactor at 80-120°C and 2.0 MPa over 8 sulfonic polystyrene-DVB ion exchange resins as catalysts (catalyst loading 0.85-3.4%). Resins swell greatly in the reaction medium and the reaction takes place mainly in the swollen gel-phase. Swollen resins in water have been characterized by analysis of ISEC data, and spaces originated in the gel phase upon swelling are described in terms of zones of different polymer density. A relationship has been found between the morphology of swollen resins and ester production. Swollen resins with low polymer density show the highest butyl levulinate yield. Dowex 50Wx2 was the most effective because it creates the largest and widest spaces in the gel-phase when swelling. Consequently, it better accommodates the proton-transfer-reaction mechanisms.

Keywords: Butyl levulinate, fructose, 5-hydroxymethylfurfural, ion-exchange resin catalysts

1. Introduction

The transformation of lignocellulose-derived sugars gives rise to valuable compounds for the refining and chemical industries called platform chemicals, such as levulinic acid (LA). The US Department of Energy has highlighted levulinic acid as a very promising platform chemical because of the number of industrially interesting LA-derived compounds [1,2]. LA production costs are expected to drop to 1 \$/kg after new upgraded biomass conversion technologies are successfully commercialized [3,4].

The most notable LA-derived compounds are alkyl levulinates (ALs). They have commercial use in mineral oil refining [5], flavoring preparations [6], latex coating compositions [7], as well as additives to polymers and perfumes [8]. Nowadays, besides its potential use as green solvents [9], levulinates are interesting as biofuels for blending with commercial gasoline or diesel to fit the quality standards settled by the Directive 2009/30/EC, a demanding European regulation on pollutant levels in exhaust

combustion gases and fuels composition [10]. This Directive sets a minimum oxygen content from biomass origin of 15% by December 31, 2020, to mitigate the greenhouse effect of vehicle exhaust emissions. Faced with the challenge of reformulating commercial fuels to meet such demanding regulations, the refining industry has realized the ALs potential for blending to commercial fuels because of their physicochemical properties and low toxicity. The levulinates of fermentation alcohols (ethanol, butanol) are 100% biofuels and, therefore, their use is very attractive. Ethyl and butyl levulinate are the most studied ALs as fuel enhancers. They have good blending octane numbers (107 and 97, respectively [11,12]), but because of their physical properties, they are more suitable for blending with commercial diesel, mostly as cold-flow enhancers. Compared to ethyl levulinate, butyl levulinate (BL) is more promising as a diesel blend component. It has a blending cetane number of about 46, close to that of commercial diesel, and it is much less soluble in water, mitigating the risk of ester separation from diesel fuel at low temperatures as an aqueous liquid phase [13,14].

Apart from a few exceptions, raw biomass or biomass-derived reactants are the starting materials to synthesize alkyl levulinates. In general, syntheses involve the treatment of reactants in alcohol and acid catalysis [15]. Synthesis of BL was undertaken for the first time in the 30s by the reaction between levulinic acid and 1-butanol (BuOH) in excess using HCl as the catalyst, although reported yields were low (40-65 %) [16-18]. Much later, in the 90s, Bart et al. proposed a kinetic model for the esterification of LA with BuOH in the presence of H₂SO₄ [19].

Acidic homogeneous catalysts present corrosion and separation problems and the industry tends to replace them with solid ones. Heterogeneously catalyzed esterification of LA with BuOH has been attempted recently, using often solid Brønsted acids: zeolites [20,21], Zr-containing MOFs [22], HPA supported on acid-treated clay montmorillonite K10 [23] and silicalite-1 [24], sulfated ZrO₂ over mesoporous silica [25], ZrO₂-based hybrid catalysts functionalized by both organosilica and HPA [26], HPA and ZrO₂ bi-functionalized organosilica nanotubes [27], WO_x/mesoporous-ZrO₂ [28], ammonium and silver co-doped phosphotungstic acid [29], Al-containing MCM-41 [30], and ion exchange resins [31,32]. In general, high ester yields are obtained using 1-butanol in excess (BuOH/LA molar ratios between 5 and 10), and moderate temperatures (60-90°C). Finally, successful attempts at BL production via immobilized enzymes are also reported [33].

As levulinic acid is quite an expensive bio-based feedstock today, some attempts have been made to produce BL directly from cellulose using both homogeneous and heterogeneous acid catalysts. Cellulose is hardly soluble in 1-butanol, and H₂SO₄ is more effective to catalyze the alcoholysis of

cellulose [34,35] than sulfonated hyperbranched polymers [36] or metal sulfates [37,38]. However, temperatures between 160 and 200°C and a very large excess of BuOH are necessary to obtain moderate ester yields (30-62%). The main drawback is the formation of a noticeably amount of soluble and insoluble polymers, called humins, because of cellulose degradation, hindering the selectivity to BL as well as the production of di-n-butyl ether (DBE) by BuOH dehydration.

To the best of our knowledge, attempts to produce BL from C₆ carbohydrates are scarce. Among the most studied monosaccharides (glucose and fructose (F)), alkyl levulinate yields are significantly higher when starting from fructose [15]. An et al. studied fructose butanolysis over metal sulfates at 190°C obtaining a BL yield of 62.8% after 2 h [37]. Kuo et al. used TiO₂ nanoparticles at 150°C and reported a BL yield of 75% after 3h [39]. Over sulfonated materials, Balakrishnan et al. reported a BL yield of 16% on Amberlyst 15 at 110°C after 30h [40]. Interestingly Liu et al. obtained BL yields of 87 and 89% on CNT-PSSA (poly (p-styrene sulfonic acid)-grafted carbon nanotubes) and Amberlyst 15, respectively, at 120°C after 24h [41]. In the mentioned works fructose conversion is high (97-100%), and the differences in yield are probably due to the presence of side reactions, as humins formation. The work of Liu et al. [41] shows that acidic ion-exchange resins are interesting catalysts. They are selective and at a moderate temperature (120°C) give better yields than TiO₂ nanoparticles at 150°C [39], and metal sulfates at 190°C [37].

Amberlyst 15 is an acidic polystyrene-divinylbenzene (PS-DVB) macroreticular resin specially designed to work in low polar organic media. However, it is often not the most suitable to work in polar environments, for example in reactions where water is produced. This resin is too stiff because of its high DVB content (20%) and swells only moderately in polar media. In alcoholic media containing water, gel-type resins are usually more active and selective catalysts than macroreticular ones with high DVB content [42,43,44]. Therefore, this paper aims to study the liquid-phase synthesis of butyl levulinate from 1-butanol and fructose over both gel-type and macroreticular sulfonic PS-DVB resins. Since the catalytic behavior of the resins is highly dependent on their morphology, tested resins have been characterized in the swollen state, and the influence of resins morphology on their catalytic activity is discussed.

2. Experimental

2.1. Chemicals

1-Butanol and D-Fructose (≥99.5%, Across Organics) were used without further purification. Butyl levulinate (≥98%, Sigma Aldrich), formic acid (≥98%, Labkem), 5-hydroxymethylfurfural, levulinic

acid, butyl formate and di-n-butyl ether ($\geq 98\%$, Across Organics), as well as distilled water, were used for analysis.

2.2. Catalysts

Eight sulfonic PS-DVB ion-exchange resins were used as catalysts. Selected resins have similar acid capacity but different morphology, including both macroreticular and gel-type ones. These resins are conventionally sulfonated (monosulfonated, having an average concentration of about a sulfonic group per styrene ring). Rohm and Haas (Amberlyst 15, Amberlyst 16, Amberlyst 39 and Amberlyst 31), Aldrich (Dowex 50Wx2, Dowex 50Wx4, and Dowex 50Wx8), and Purolite (CT124) supplied tested catalysts. Table 1 shows the properties of these resins.

Table 1. Properties of the resin catalysts used

Catalyst	Acronym	Morphology ^a	DVB% ^b	Acid capacity (mmol H ⁺ /g) ^c	Native particle size range (mm) ^d	T _{max} (°C) ^e
Dowex 50Wx2	DOW2	G	2	4.98	0.074 – 0.149	150
Dowex 50Wx4	DOW4	G	4	4.95	0.074 – 0.149	150
Amberlyst 31	A31	G	4	4.84	0.309 – 1.143	130
CT124	CT124	G	4	5.00	0.425 – 1.200	130
Dowex 50Wx8	DOW8	G	8	4.83	0.074 – 0.149	150
Amberlyst 39	A39	M	8	4.82	0.410 – 1.141	130
Amberlyst 16	A16	M	12	4.80	0.410 – 0.948	130
Amberlyst 15	A15	M	20	4.81	0.310 – 1.041	120

^a Macroreticular (M) and gel-type (G)

^b From Bringué et al. [42]

^c Titration against standard base following the procedure described by Fischer and Kunin [45]

^d Particle size distribution of the commercial sample (1-99% volume fraction)

^e Maximum operating temperature. Information supplied by the manufacturer

2.3. Apparatus and analysis

Experiments were carried out in a 100-mL stainless steel reactor (MagneDrive II, Autoclave Engineers). The reactor was heated by an electric oven TC 22 Pro 9, and its temperature was controlled to $\pm 0.1^\circ\text{C}$ by a TIC controller TOHO TIM-125. The reaction medium was stirred by a magnetic drive turbine equipped with a 4-blade axial-up mixer. The dried catalyst was injected into the reactor from an external cylinder by shifting with N₂.

Liquid samples were taken hourly out of the reactor and analyzed. Butyl levulinate, butyl formate (BF), 5-butoxymethylfurfural (BMF), di-n-butyl ether, and water were determined by Gas-Liquid

Chromatography. An Agilent HP6890 GLC apparatus equipped with a TCD detector and an HP Pona methyl silicone capillary column HP190195-001 (50 m x 0.2 mm x 0.5 μ m) analyzed 0.2 μ L liquid aliquots. A temperature ramp of 10°C/min from 50°C up to 250°C was initially programmed and then held for 6 min. He (\geq 99.998%, Linde) was the carrier gas at a column flow rate of 1 mL/min. Fructose, formic acid (FA), levulinic acid, and 5-hydroxymethylfurfural (HMF) were determined by High-Performance Liquid Chromatography. An Agilent 1200 Infinity II HPLC equipped with a Refractive Index (RI) detector and Agilent Hi-Plex H column (300 mm x 7.7 mm) analyzed 100 μ L liquid aliquots. The mobile phase was a 0.005N aqueous solution of H₂SO₄ at a flow rate of 0.6 mL/min and the column temperature 50°C. Reaction products were identified by an Agilent GC/MS (6890A series GLC with an Agilent GC/MS 5973 detector, and chemical database software).

2.4. Methodology

Dowex 50Wx2, Dowex 50Wx4, and Dowex 50Wx8 resins were used as 100 – 200 mesh beads (0.074-0.149 mm) as shipped. Commercial beads of Amberlyst 15, Amberlyst 16, Amberlyst 39, Amberlyst 31, and CT124 were crushed and sieved, and 0.08-0.1 mm particles were selected. Catalysts were dried at 110°C for 2h at atmospheric pressure and then at 10 mbar overnight. The residual water of the resins, determined with a Volumetric Karl Fischer Titrator Orion AF8 (Thermo Electron Corporation), was less than 3 wt.%.

Since the solubility of fructose in alcohol is limited [15], the solubility of fructose in 1-butanol has been determined at 25, 80, and 100°C by a gravimetric method following the experimental procedure described elsewhere [46]. Solubility at 25°C is very low (2.60 g/L). Solubility increases highly with temperature and it is 37.7 g/L at 80°C. At 100°C solubility is about 270 g/L, but liquid becomes pale yellow probably due to the thermal decomposition of fructose.

Experiments were performed at 80-120°C. In a typical experiment, a mixture of 1-butanol (60 mL) and water (10 mL) containing 1.5 g of fructose was charged into the reactor (initial molar ratio 1-butanol/fructose, $R_{\text{BuOH}/\text{F}} = 79$; fructose concentration 0.142 mol/kg). Water and 1-butanol are partly miscible. Solubility of water in the butanol-rich region is 20.4 wt.% at 25°C [47], 30.6 wt.% at 90°C [47], and 50 wt.% at 120°C [48]. As the liquid mixture contained 17.2 wt.% of water (1-butanol/water molar ratio, $R_{\text{BuOH}/\text{W}} = 1.19$), it was not separated into two phases. Furthermore, despite fructose reduces water solubility in 1-butanol, a 0.142 mol/kg solution of fructose in water-saturated 1-butanol does not form clouds in the range 25-80°C [49]. As the water solubility increases with temperature it is assured that the solution is homogeneous up to 120°C.

The reactor was stirred at 500 rpm, set at 2 MPa to maintain the liquid phase over the reaction, and heated. When the liquid reached the desired temperature, dried catalyst (0.5-2 g; catalyst loading 0.85-3.4 %) was injected into the reactor. Catalyst injection was taken as time zero. 8h-experiments were carried out.

In each experiment, fructose conversion (X_F), and yield of fructose towards the product j (Y_F^j) were estimated by Eqs. 1 and 2, respectively

$$X_F = \frac{\text{mole of } F \text{ reacted}}{\text{mole of } F \text{ initially}} \times 100 \text{ [\%, mol/mol]} \quad (1)$$

$$Y_F^j = \frac{\text{mole of } F \text{ reacted to form } j}{\text{mole of } F \text{ initially}} \times 100 \text{ [\%, mol/mol]} \quad (2)$$

Replicated runs were made for some experiments and the reproducibility of results was found to be reliable. Fructose conversions were accurate within $\pm 1\%$. On the other hand, BL yields were accurate within $\pm 5\%$ and those of HMF, BMF, and LA within $\pm 5-8\%$

2.5. Reused catalyst

The recovered resin was washed in a 25-mL column by percolation with deionized water to remove solid materials present in the used catalyst. To assure that the resins were completely swollen, the column was filled with water, and 2-BV (bed volume) of water was poured into the column at 4 BV/h. This procedure was repeated until the poured water was colorless. After that, the resin was downwash with methanol three times to remove all the water. Finally, the catalyst was dried as explained before. Its final water content was less than 3 wt.% (Karl Fischer titration).

3. Results and discussion

3.1 Blank experiments

Blank experiments with a 1-butanol/water mixture ($R_{BuOH/W} = 1.19$) containing 1.5 g of fructose were carried out at 120°C without a catalyst. Fructose undergoes thermal decomposition, with $X_F \approx 20\%$ after 8h. HMF was the only product observed with a yield of 8.8%. The difference between fructose conversion and HMF yield suggests the formation of a small number of byproducts by thermal decomposition of fructose, although below the detection limits of HPLC and GLC analyses. This fact is in line with blank experiments with fructose (9 wt. %) in 0.5 mL of water/GVL mixture (50:50 v/v) performed by Thapa et al., who quoted $X_F \approx 20\%$ and $Y_F^{HMF} = 7\%$ after 24 h at 120°C [50]. In contrast, 1-butanol does not undergo reaction under the specified reaction conditions since neither DBE nor butenes were detected.

3.2. Analysis of a model experiment with Dowex 50Wx2

It is found in the open literature that in alcoholic media containing water, gel-type resins with low DVB content are usually effective catalysts [42,43,44], thus Dowex 50Wx2 resin (gel-type, with 2% DVB) was selected. Figure 1 shows the variation in the mole number of fructose and reaction products over time in an experiment performed at 120°C. It is seen that fructose decomposes readily and its conversion is almost complete after 4h. HMF forms swiftly from the beginning of the reaction reaching a maximum at about 1 h. Then the HMF amount decreases continuously and the HMF yield is only about 3.8% after 8h. The yield of BMF, LA, BL, and BF increases steadily over time, although that of BMF seems to reach a smooth maximum at about 7 h ($Y_F^{BMF} = 32.6\%$). The yield of butyl levulinate at 8h is 32.3%.

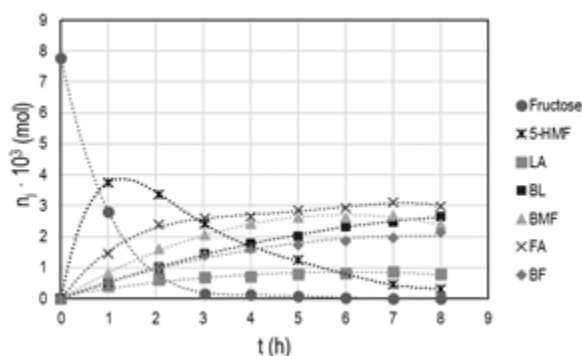


Figure. 1. Moles of fructose, HMF, BMF, LA, BL, FA, and BF vs. time on Dowex 50Wx2 ($T = 120^\circ\text{C}$; $R_{\text{BuOH}/F} = 79$; $R_{\text{BuOH}/W} = 1.19$; 1g dried catalyst; catalyst loading 1.7 wt. %)

The process for producing butyl levulinate from fructose takes place through a complex series-parallel reaction scheme (Figure 2) where [15,51]:

- 1) Fructose dehydrates firstly to HMF
- 2) HMF reacts with 1-butanol to give BMF. The subsequent alcoholysis of BMF yields BL and BF
- 3) HMF rehydrates to LA giving place to FA as a coproduct. Subsequently, both acids esterify to BL and BF, respectively.

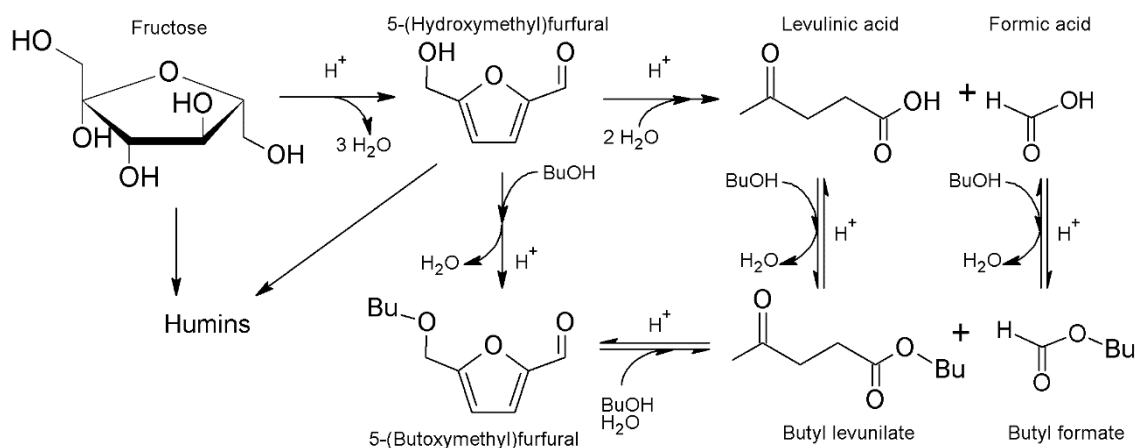


Figure 2. Reaction scheme [15,51]

According to the stoichiometry of the involved reactions, the sum of FA and BF moles (reaction coproducts) should be the same as that of LA and BL, within the limits of the experimental error. However, as seen in Figure 1, the sum of moles of FA and BF is higher by 1.49 times at the end of the experiment. The fact that solvolysis of carbohydrates gives place to a molar excess of FA (plus BF) over LA (plus BL) is often reported in the presence of acid catalysts [50,52-55] although it is not well understood. At least four potential pathways, depending on reaction conditions, have been quoted as responsible for the formation of the FA excess in the hydrolysis of biomass-derived hexoses: through D-erythrose, furfuryl alcohol, furfural, or pyruvaldehyde formation [52]. FA is formed as well as D-erythrose, furfuryl alcohol, furfural, or pyruvaldehyde in all four pathways. However, we do not have detected any of those substances, probably because they were below the detection threshold of the GLC and HPLC apparatus due to the small initial amount of fructose. Furthermore, they are unstable and could probably react quickly giving place to polymers contributing this way to the formation of humins.

At the end of the experiment, the liquid is brown. The molar balance of fructose shows that about 80% of carbohydrate has been converted into HMF, BMF, LA, and BL, which implies that some fructose decomposes forming humins. Correspondingly, the balance of fructose carbon atoms shows that about 17% are lost. Humins formation is currently attributed to degradation reactions of fructose [52], HMF [56], LA [50], and cross-reaction between fructose and HMF [57]. It is to be noted that compounds such as pyruvaldehyde, furfuryl alcohol, or furfural, are unstable and react easily forming polymers or humins. The pathways to produce humins from HMF are not so clear. It has been hypothesized that soluble humins are formed by condensation/etherification of HMF, and

insoluble humins by HMF addition (polymerization) [56]. Solid humins are retained in the catalyst, and soluble ones remain in the solution.

A large amount of BMF remains in the liquid phase after 8h of reaction ($Y_F^{\text{BMF}} = 29.3\%$). Since 1-butanol is in large excess, BL yield is expected to increase substantially over time as BMF alcoholysis and LA esterification occur.

The molar balance of 1-butanol was fulfilled within $\pm 0.5\%$. No DBE was detected despite the large excess of BuOH in the reaction medium, in agreement with the study of 1-butanol dehydration to di-n-butyl ether on ion-exchange resins by Pérez et al. [44], who showed the low catalytic activity of acidic resins in the dehydration of 1-butanol to DBE at 120°C in the presence of water.

3.3. Effect of catalyst mass of Dowex 50Wx2 and temperature

The effect of the catalyst mass of Dowex 50Wx2 was checked at 120°C by changing the mass of dried resin between 0.5 and 2 g. Figure 3 shows the curves of fructose conversion and yield of HMF, LA, BMF, and BL as a function of contact time ($t \cdot W/n_F^0$). As can be seen, X_F and yield curves obtained with different catalyst mass practically overlap, which confirms the reliability of data and that the reactor was not saturated with the solid catalyst. As the initial composition of the reactor is the same, and the reaction scheme is a series-parallel one, the contact time increases on increasing the catalyst mass, and consequently, the system moves to the production of butyl levulinate. Figure 3E shows that BL yield rises to 43.5% when contact time is about 1900 g·h/mol. At such a long contact time, HMF is almost consumed ($Y_F^{\text{HMF}} \approx 1.5\%$, Fig. 3B). As seen in Fig. 3D, BMF yield over contact time has a maximum according to its role as an intermediate compound in the reaction scheme. However, the amount of BMF at 1900 g·h/mol is still considerable and BL production is expected to increase even more as BMF is consumed. The production of LA (Fig. 3C), FA, and BF (not shown), like that of BL, rise moderately. Finally, it is to be noted that DBE was detected only in the experiment with 2g of catalyst at very long contact time.

Figure 4 shows fructose conversion and yield of HMF, LA, BMF, and BL over time as a function of temperature in the range 80-120°C. As expected, X_F increases with temperature (Fig. 4A). At 100°C it is higher than 99.5% at 8h reaction, and at 110°C at 4h. Accordingly, product formation accelerates with temperature. Regarding HMF formation, Y_F^{HMF} increases continuously at 80 and 90°C whereas yield curves at 100-120°C show a maximum (Fig. 4B). The maximum value is smaller, and it appears at shorter times as temperature increases, since HMF transformation into products is faster. At 80°C, decomposition of HMF is very slow, and only LA (Fig. 4C) and FA (not shown) are formed. Therefore,

the hydrolysis of HMF takes place already at 80°C. The formation of BMF is observed at 90°C after 6 h (Fig. 4D). BMF yield increases with temperature, and it shows a maximum at 120°C, according to its role as an intermediate compound in the series-parallel reaction scheme (Fig. 2). Finally, BL (Fig. 4E) and BF (not shown) are observed at 100°C and 3h. The alcoholysis of BMF is, therefore, active at 100°C. The production of BL, BF, LA, and FA increases with temperature, and the esters appear at shorter reaction times. By comparing the formation of LA and BMF it can be inferred that the hydrolysis mechanism predominates at the lower temperature of the range explored (80°C), and alcoholysis at the highest one (120°C).

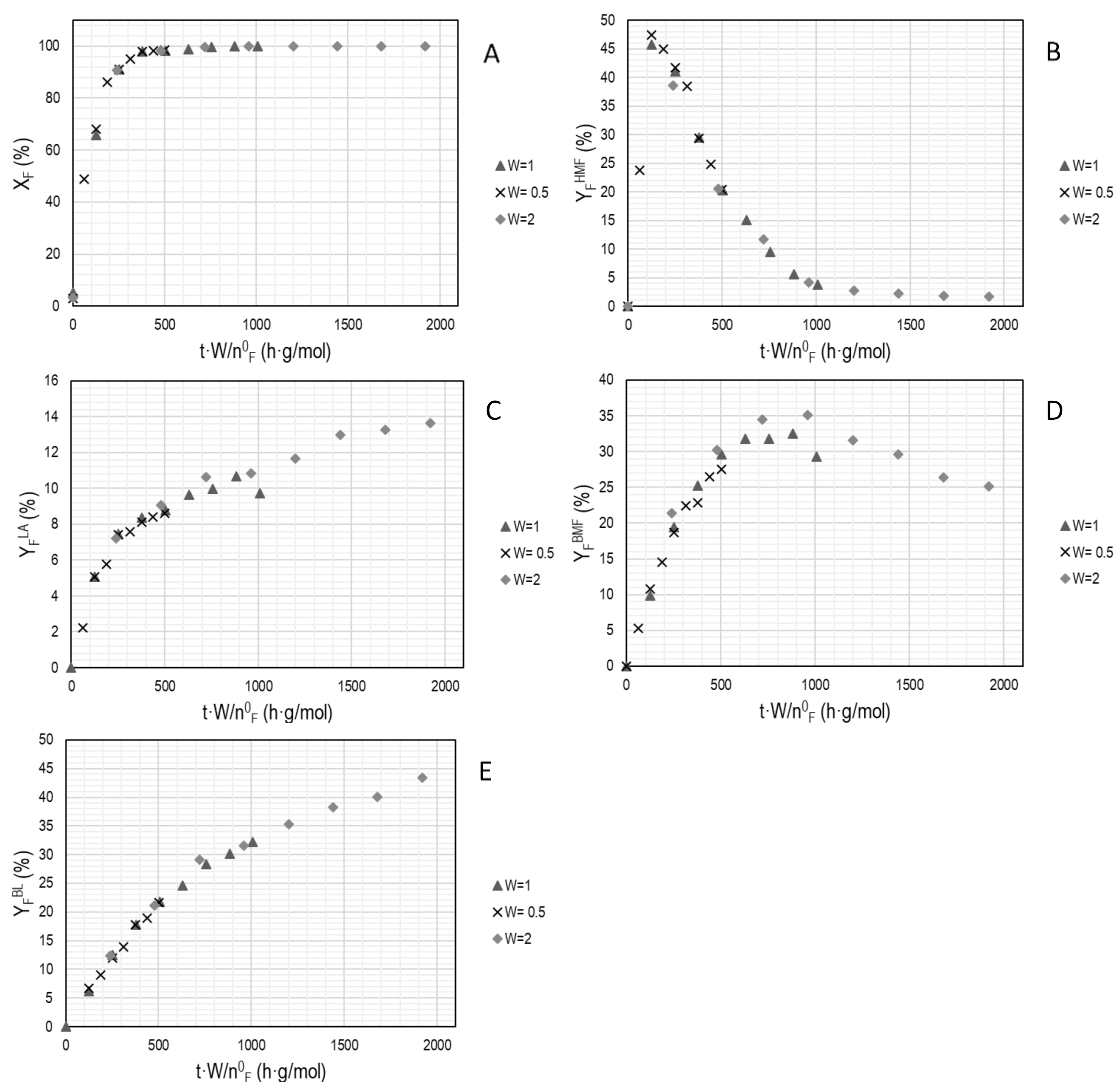


Figure 3. Fructose conversion (A) and yield of HMF (B), LA (C), BMF (D), and BL (E) over contact time as a function of catalyst mass (Dowex 50Wx2; $T = 120^\circ\text{C}$; $R_{\text{BuOH}/F} = 79$; $R_{\text{BuOH}/W} = 1.19$).

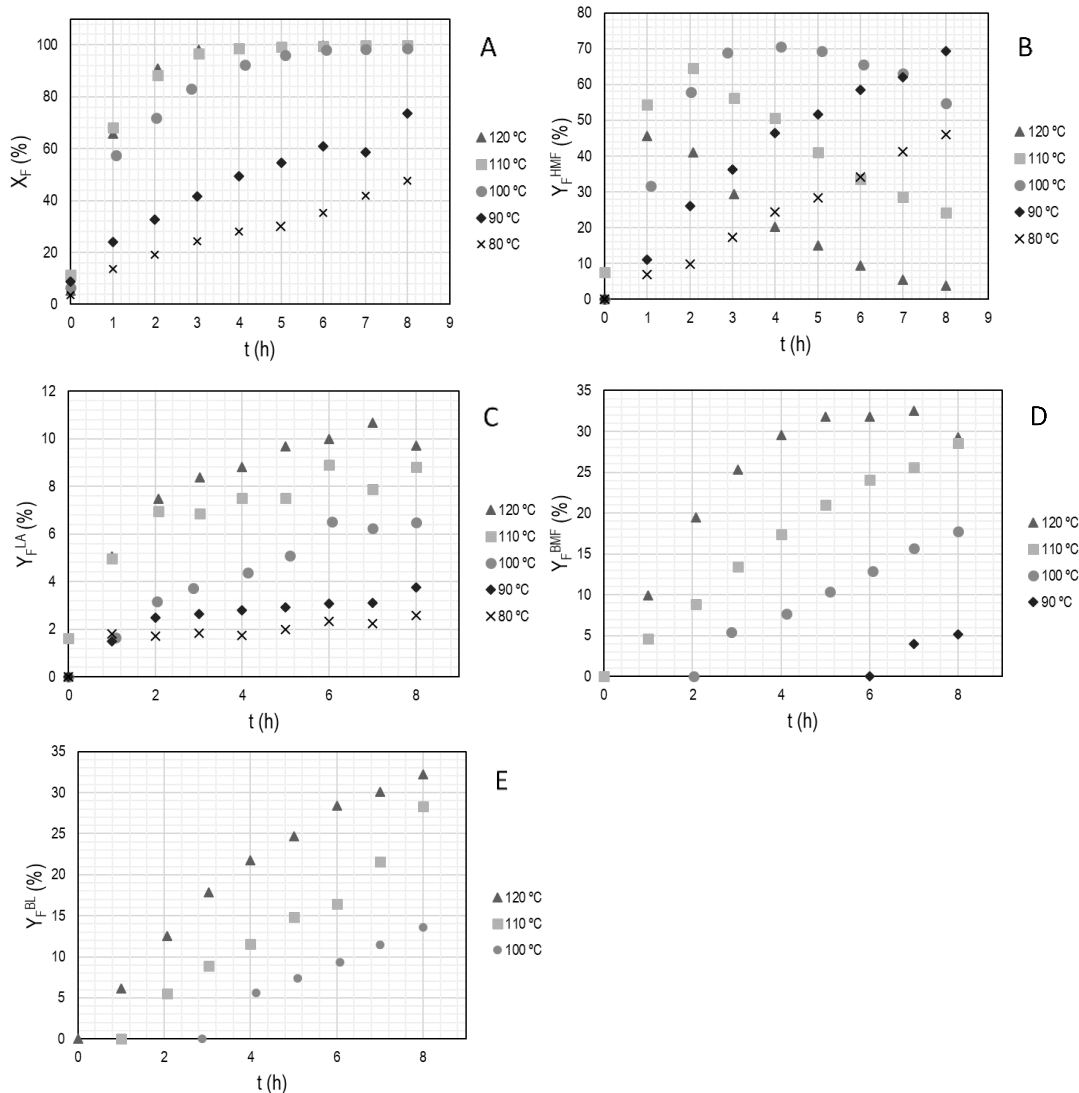


Figure 4. Fructose conversion (A) and yield of HMF (B), LA (C), BMF (D), and BL (E) vs. time as a function of temperature (Dowex 50Wx2; $R_{BuOH/F} = 79$; $R_{BuOH/W} = 1.19$; 1g dried catalyst; catalyst loading 1.7 wt. %)

3.4. Assessment of the resistance to mass transfer in Dowex 50Wx2 resin

The influence of external and intra-particle mass transfer resistance was checked in the experiment performed at 120°C and 1 g of dried Dowex 50Wx2. As a general rule, mass transfer resistance is reduced to negligible proportions at moderate temperatures if sufficiently small catalyst particles are used and the reaction rate is not high. Since the reaction network is complex, resistance to mass transfer was checked at zero time examining the rate of fructose consumption. Assuming steady state, the rate of fructose consumption in the resin bead, $-r_F^0$, may be written in terms of the diffusion rate of fructose from the bulk liquid to the surface as [58]:

$$-r_F^0 = k_{m,F} a_m (C_{F,b} - C_{F,s}) \quad (3)$$

where $k_{m,F}$ is the fructose mass-transfer coefficient between bulk liquid and the solid external surface, a_m is the external surface area per unit mass of the particle, $C_{F,b}$ is the fructose concentration in the bulk liquid, and $C_{F,s}$ the fructose concentration in the resin external surface, respectively. As can be seen in Table 2, the fractional concentration difference $(C_{F,b} - C_{F,s})/C_{F,b}$ is less than 0.2%. Consequently, the resistance to external mass transfer is negligible.

Since the influence of external mass transfer is negligible, the criterion for observing chemically controlled reaction rates is that the Weisz-Prater modulus, in terms of measurable quantities, should be [59]:

$$\Phi = \frac{(-r_F^0) \rho_P L_e^2}{D_{e,F} C_{F,S}} < 1 \quad (4)$$

where L_e is the effective diffusion-path-length parameter (a third of the radius for spherical beads), ρ_P is the apparent density of the particle, and $D_{e,F}$ is the effective diffusivity of fructose in catalyst pores, m^2/h . As seen in Table 2, $\Phi = 0.002$. Consequently, the reaction rate is also free of intra-particle mass transfer resistance. The detailed procedure followed to estimate both the fractional concentration difference and the Weisz-Prate modulus is described in the SI section.

Table 2. Fructose fractional concentration difference between bulk liquid and catalyst surface and Weisz-Prater modulus (T = 120°C; $R_{BuOH/F} = 79$; $R_{BuOH/W} = 1.19$; 1g dried Dowex 50Wx2; 500 rpm)

Parameter	Value
$-r_F^0$ (mol/h·g) ^a	$5.0 \cdot 10^{-3}$
a_m (m ² /g) ^b	0.0243
$k_{m,F}$ (m/h) ^c	1.2
$(C_{F,b} - C_{F,s})/C_{F,b}$	0.0017
ρ_P (kg/m ³) ^d	306
L_e (m)	$2.88 \cdot 10^{-5}$
$D_{e,F}$ (m ² /s) ^e	$2.30 \cdot 10^{-9}$
$C_{F,S}$ (mol/m ³)	103
Φ	0.0020

^a Obtained from the function of variation of fructose conversion against time.

^b For an spherical particle, $a_m = 6/\rho_P \bar{d}_P$, with ρ_P = apparent density of the resins and \bar{d}_P = mean particle diameter

^c Estimated by using the correlation of Sano et al. [60]

^d $\rho_P = \rho_S(1 - \theta)$. ρ_S is the skeletal density [42], and θ the porosity of the catalyst

^e Estimated by a modified Wilke-Chang equation [61]

3.5. Catalyst screening

A series of experiments was performed using 8 acidic resins at 120°C with a 1-butanol/water mixture ($R_{\text{BuOH/W}} = 1.19$) containing 1.5 g of fructose. In all the experiments 1 g of dried catalyst was used. Tested resins were gel-type (Dowex 50Wx2, Dowex 50Wx4, Amberlyst 31, CT124, and Dowex 50Wx8) and macroreticular (Amberlyst 39, Amberlyst 16, and Amberlyst 15). All the resins have a very similar acid capacity. As described in Section 2.4, catalyst particle size distribution was 0.074 – 0.149 mm (average 0.105 mm) for Dowex resins and 0.08 - 0.1 mm (average 0.089 mm) for the other. The stirring rate was fixed at 500 rpm. Under such operating conditions and small particles, the influence of mass transfer was negligible for all the resins as shown in detail in the SI section.

All catalysts were active producing BL from fructose but important differences in their catalytic behavior are seen depending on the resin structure (gel-type or macroreticular) and the crosslinking degree (percentage by weight of DVB in the mixture of styrene and DVB copolymers that gives rise to the resin). Figure 5 shows the conversion of fructose and the yield of HMF, LA, BMF, BL, FA, and BF over time. For the sake of clarity, only the results of three catalysts are presented in Figure 5: the gel-type resin Dowex 50Wx2 (2%DVB), the low-crosslinked macroreticular resin Amberlyst 39 (8%DVB), and the high-crosslinked macroreticular resin Amberlyst 15 (20%DVB).

As Fig. 5A shows, fructose reacts completely irrespective of the catalyst used. Although some fructose is decomposed thermally as seen in section 3.1, the presence of a catalyst accelerates the conversion of the monosaccharide into HMF and humins. It is seen that fructose conversion on Dowex 50Wx2 and Amberlyst 39 is similar at any time, but it is initially slower on Amberlyst 15.

Fig. 5B shows the variation of HMF yield over time. HMF forms fast, and subsequently, it rehydrates giving place to LA and etherifies to BMF. Curves of HMF yield show a maximum. Dowex 50Wx2 reaches that maximum at about 1h, Amberlyst 39 does it between 1 and 2 h, and Amberlyst 15 at 2h. Clear differences are seen at the end of the runs: HMF yield at 8h is 3.8% on Dowex 50Wx2, about 10% on Amberlyst 39, and 36% over Amberlyst 15, respectively. However, interpretation of HMF yield curves is not easy, since HMF also forms humins through several mechanisms, and humins formation from HMF is more noticeable at the higher HMF concentration [57].

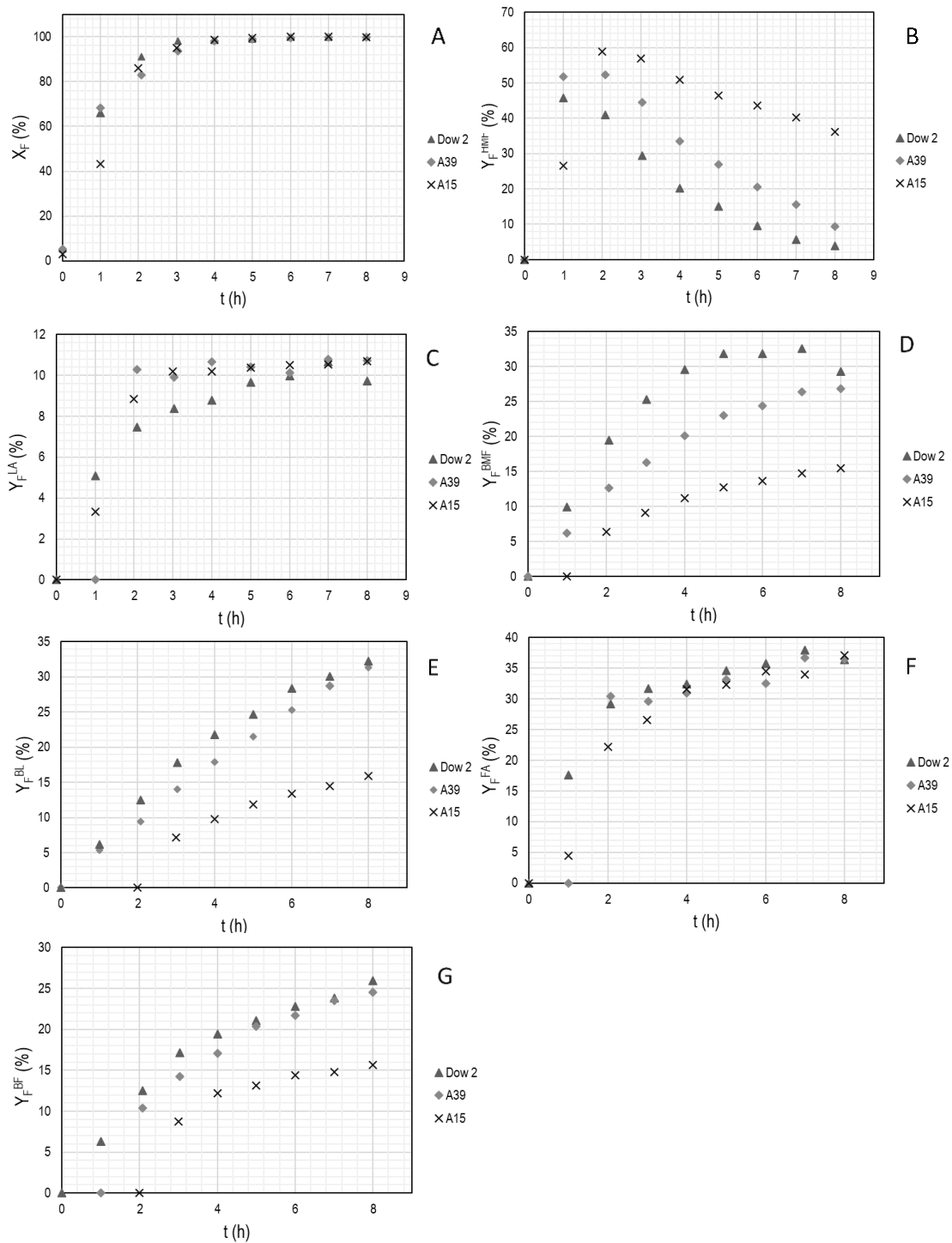


Figure 5. Fructose conversion (A) and yield of HMF (B), LA (C), BMF (D), BL (E), FA (F), and BF (G) vs. time on DOW2, A39, and A15 ($T = 120^{\circ}\text{C}$, $R_{\text{BuOH/F}} = 79$; $R_{\text{BuOH/W}} = 1.19$; 1g dried catalyst; catalyst loading 1.7 wt. %)

HMF produces butyl levulinate via the hydrolysis and alcoholysis pathways. Hydrolysis of HMF gives rise firstly to LA, whereas alcoholysis requires the etherification of HMF to BMF. As seen in Figs. 5C and 5D, LA yield is lower than that of BMF. So, it can be inferred that etherification to BMF is a faster reaction and the alcoholysis pathway predominates over hydrolysis at 120°C with all catalysts. As seen in Fig. 5C, LA yield is similar over the three resins. However, the BMF yield on Dowex 50Wx2 is higher than those of Amberlyst 39 and Amberlyst 15 (Fig. 5D). It is to be noted that BMF is detected at 2h of reaction on Amberlyst 15, whereas it is formed at the beginning of the reaction on the other two catalysts

Butyl levulinate is formed by the esterification of LA and by the etherification of BMF. As can be seen in Fig. 5E, whereas Dowex 50Wx2 and Amberlyst 39 have similar BL yields, and even show very close values at 8h (about 33%), BL is detected on Amberlyst 15 at 3h, and the BL yield is only of 15% at 8h

Finally, Figs. 5F and 5G show the yield of FA and BF. As seen in Fig. 5F, FA yields differ at the beginning of the reaction, but they are very similar in the three resins from 4h. In contrast, BF formation shows a similar picture to the BMF yield. Dowex 50Wx2 and Amberlyst 39 have similar BF yields at 8h (about 25%), and on Amberlyst 15 it is detected at 3h with a yield of 15% at 8h. It is to be noted that DBE was not detected in any experiment of this series.

It is seen that although fructose conversion is fast, the yield of HMF, BMF, BL, and BF is different on Dowex 50Wx2, Amberlyst 39, and Amberlyst 15. The formation of BMF, BL, and BF is lower over Amberlyst 15, the resin with the higher DVB content and consequently the stiffest one. At the same time, HMF yield shows the opposite trend: the higher yield at 8h is found on Amberlyst 15. Although LA and FA yield is of the same order on the three catalysts, it can be inferred that the actual morphology of resins in the reaction medium plays an important role in butyl levulinate production.

3.6. Influence of the acid site density of swollen resins on catalytic activity

Table 3 shows the yield of butyl levulinate and the other reaction products at 6h. As seen in Fig. 5, fructose conversion is higher than 99.5% on all the catalysts. The highest BL yield is obtained on Dowex 50Wx2 and the lowest on Amberlyst 15. As a whole, BL and BMF yield decrease in the order: gel-type resins with 2% DVB (Dowex 50Wx2), 4% DVB (Dowex 50Wx4, CT124, Amberlyst 31) and 8% DVB (Dowex 50Wx8), and macroreticular ones with 8% DVB (Amberlyst 39), 12% DVB (Amberlyst 16) and 20% DVB (Amberlyst 15). On the contrary, HMF yield follows the opposite trend, since the highest HMF yield is obtained on Amberlyst 15, and the lowest on Dowex 50Wx2. BF yield is approximately the same on all catalysts, within the limits of the experimental error, but Amberlyst 16

and Amberlyst 15, which show lower values. As for LA and FA, the yield is similar over all the resins; FA yield being much higher than that of LA. The fact that the formation of the bulkiest molecules of the reaction system was related to the resin type and their crosslinking degree suggests that the reactions take place mainly within the resin gel-phase.

Table 3. Yield of HMF, LA, BMF, BL, FA, and BF on tested catalysts at 6 h ($T=120^{\circ}\text{C}$, $R_{\text{BuOH}/\text{F}}=79$; $R_{\text{BuOH}/\text{W}}=1.19$; 1g dry catalyst; catalyst loading = 1.7 wt. %). $X_{\text{F}} > 99.5\%$ on all resins

Catalyst	DVB (%)	$Y_{\text{F}}^{\text{HMF}}$ (%)	Y_{F}^{LA} (%)	$Y_{\text{F}}^{\text{BMF}}$ (%)	Y_{F}^{BL} (%)	Y_{F}^{FA} (%)	Y_{F}^{BF} (%)
Dowex 50Wx2	2	9.49±0.45	10.0±0.5	31.8±1.4	28.4±1.2	35.7±1.6	22.8±1.2
Dowex 50Wx4	4	12.7±0.3	11.1±0.2	27.6±1.5	27.1±1.4	36.2±1.5	22.7±1.45
Amberlyst 31	4	15.3	13.5	22.3	22.8	34.2	20.8
CT124	4	10.6	5.45	23.2	23.1	31.4	20.1
Dowex 50Wx8	8	19.3	12.3	20.8	24.2	36.3	22.5
Amberlyst 39	8	20.5	10.1	24.4	25.3	32.6	22.0
Amberlyst 16	12	34.5	13.5	15.1	17.7	35.8	18.8
Amberlyst 15	20	43.6	10.5	13.7	13.4	34.5	14.4

Ion exchange resins swell in polar media. Table 4 shows the mean particle size of tested resins determined by laser measurements in air, water, and 1-butanol with a Beckman Coulter LS Particle Size Analyzer. As seen, resins greatly swell both in water and in 1-butanol, although they swell more in water. In general, swelling decreases in the order: gel-type resins with 2, 4, and 8% DVB, and macroreticular ones with 8, 12, and 20 % DVB.

Table 4. Mean particle size of commercial catalysts determined by laser measurements in air, water, and 1-butanol and swelling in water and 1-butanol

Catalyst	Native particle size range (mm)	Mean particle diameter (μm)			Swelling ratio ^a (%)	
		Air	Water	1-Butanol	Water	1-Butanol
Dowex 50Wx2	0.147 – 0.296	252	451	383	473	250
Dowex 50Wx4	0.074 – 0.149	118	163	154	165	122
Amberlyst 31	0.309 – 1.143	507	720	660	186	121
CT124	0.425 – 1.200	758	1194	1110	291	214
Dowex 50Wx8	0.074 – 0.149	167	235	212	178	104
Amberlyst 39	0.410 – 1.141	540	768	724	188	141
Amberlyst 16	0.410 – 0.948	562	690	630	87	40
Amberlyst 15	0.310 – 1.041	650	741	729	48	21

^a Swelling ratio: quotient between the increase in the volume of a particle swollen in water or 1-butanol and the volume of the dry particle

Resins undergo a series of morphological changes on swelling, by which spaces that did not exist in the dry state appear (Fig. 6). Dried gel-type resins contain only micropores (spaces between the polymer chains). Mesopores appear when they swell in polar media (water, alcohol...), and disappear on shrinking in non-polar media. Macroreticular resins can be described as a collection of polymeric gel-phase microspheres interspersed by permanent pores. In a non-polar medium, these resins have macro and mesopores (between the aggregates of microspheres) and micropores (inside gel-type microspheres). As a result of swelling, an additional number of macro and mesopores appear, spaces that existed in the gel-phase in the range of micropores slightly increase their size, and at the same time, new spaces are formed within the gel phase.

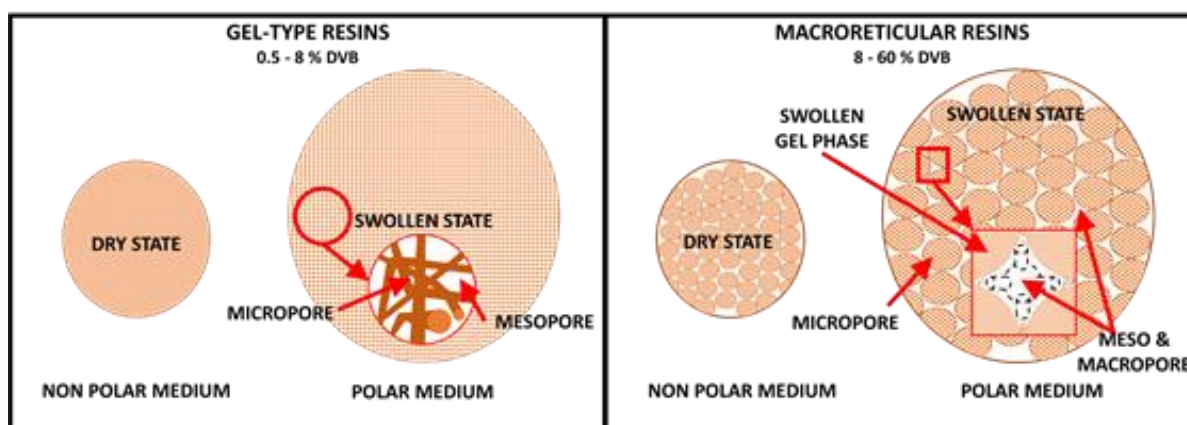


Figure 6. Morphological changes of gel-type and macroreticular resin particles due to swelling in polar media

The spaces formed on swelling are difficult to characterize because they are highly dependent on the medium polarity. An added difficulty is a consequence of the non-homogeneity of the gel-phase. However, a good picture of the spaces formed on swelling can be obtained from the analysis of elution data of solutes of different molecular weight in an aqueous solution using the ISEC technique (Inversion Steric Exclusion Chromatography) technique, as proposed by Jerabek [62-64]. He modeled the porous resin as a set of discrete fractions, each composed of pores having simple geometry and uniform sizes. Macro and mesopores are described by the cylindrical pore model in terms of pore surface and volume [63]. Micropores are described in terms of the Ogston model as spaces between randomly oriented rigid rods [65]. The relevant parameter of the model is V_{sp} , the specific volume of swollen resins (pores + polymer skeleton). The Ogston model also allows distinguishing between

zones of different polymer density in the swollen gel phase (in terms of total rod length per volume unit of the swollen polymer, nm/nm³).

Table 5. Morphology of tested resins in the dry state and swollen in water.

Catalyst	Dry state			Swollen in water (from ISEC data)			
	S_g (m ² /g) ^a	V_g (cm ³ /g) ^a	d_{pore} (nm) ^c	ΣS_{pore} (m ² /g) ^b	ΣV_{pore} (cm ³ /g) ^b	d_{pore} (nm) ^c	ΣV_{sp} (cm ³ /g)
Dowex 50Wx2							2.677
Dowex 50Wx4							2.061
Amberlyst 31							2.096
CT124							2.006
Dowex 50Wx8							1.404
Amberlyst 39	0.09	3x10 ⁻⁴	17.6	56	0.155	15.0	1.643
Amberlyst 16	1.69	0.013	29.7	46	0.188	15.5	1.136
Amberlyst 15	42.0	0.328	31.8	192	0.616	12.4	0.622

^a By N₂ adsorption-desorption at 77K. Surface area from BET method (S_g), and pore volume at $P/P_0 = 0.99$ (V_g).

^b Surface (ΣS_{pore}) and volume (ΣV_{pore}) of mesopores in the swollen state.

^c Mean pore diameter

Note: The porosity of the swollen resins is $\theta = (\Sigma V_{pore} + \Sigma V_{sp} - 1/\rho_s) / (\Sigma V_{pore} + \Sigma V_{sp})$

As Table 5 shows, pore surface and volume in macroreticular resins increase on swelling, and mean mesopore diameter is in the range 12-15 nm, large enough to make easier the access to the gel-phase surface. Gel-type resins, which do not have mesopores in the dried state, do not generate spaces that can be characterizable with the cylindrical pore model. However, new spaces are formed within the gel-phase of the macroreticular and gel-type resins when swelling in water. Table 5 shows that the total specific volume of swollen resins (ΣV_{sp}) highly varies from Dowex 50Wx2 to Amberlyst 15. Typically, gel-type resins show higher ΣV_{sp} values than macroreticular ones and, among each resins group, ΣV_{sp} decreases as DVB% increases. The distribution of zones of different density of the tested resins is seen in Figure 7. Gel-type resins with 2-4% DVB and macroreticular ones with 8% DVB show chain concentrations in swollen gel-phase of 0.4-0.8 nm/nm³, typical of slightly dense polymer mass. Gel-type resins with 8% DVB and medium and highly crosslinked macroreticular ones show polymer densities in the range 0.8-1.5 nm/nm³, typical of highly dense polymer mass. Equivalent pore diameter of spaces in polymer zones with chain density 0.1 nm/nm³, 0.2 nm/nm³, 0.4 nm/nm³, 0.8 nm/nm³ and 1.5 nm/nm³ are 9.3 nm, 4.8 nm, 2.6 nm, 1.5 nm and 1.0 nm, respectively [66]. Highly swollen resins, e.g. Dowex 50Wx2, have a very high ΣV_{sp} value (large pore volume within gel-phase)

and low polymer density. As a result, such resins have a very flexible polymer network and can accommodate a greater number of bulky molecules. On the contrary, low swollen resins, e.g, Amberlyst 15, have low ΣV_{sp} value (small pore volume within the gel-phase) and a high polymer density. Therefore, they have a stiffer polymer network, contain fewer molecules in the open spaces and bulky molecules tend to be excluded

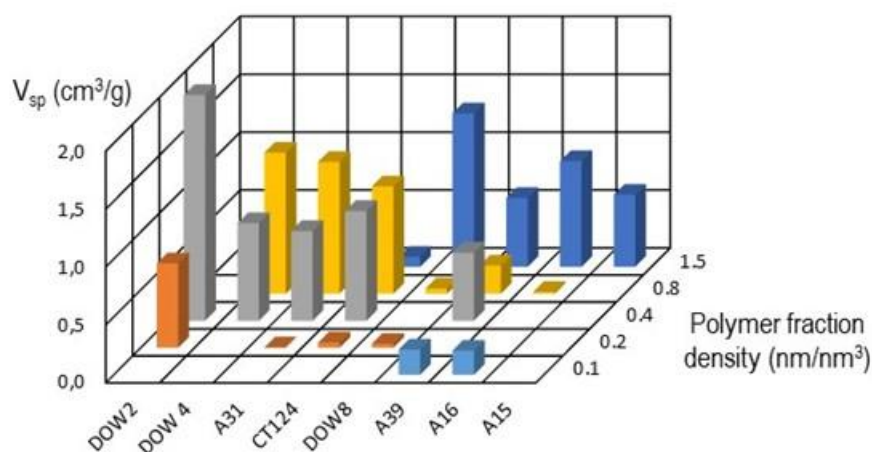


Figure 7. Distribution of zones of different polymer density of swollen PS-DVB catalysts determined from ISEC data analysis in aqueous solution

An indication that a resin zone with polymer chains concentration C (length of rods per total volume unit, pores + polymer skeleton) is accessible to spherical molecules of diameter d_m is given by the Ogston distribution coefficient, K_0 , defined as [64]:

$$K_0 = \exp\left(-0.25\pi C(d_m^2 + d_c^2)\right) \quad (5)$$

The diameter of randomly distributed rigid rods representing polymer chains is d_c . K_0 ranges from 1 (the concentration of a given compound is the same as outside the gel-phase) to 0 (the compound is excluded from the gel phase). Eq. 5 considers spherical molecules, consequently, the length is a good estimate of their effective size, d_m . Molecular lengths were computed with Chem3D 18.0 software (ChemOffice) using the MM2 computational engine. First, the energy of the structure was minimized, and then molecular dynamics calculations were performed at 120°C. Table 6 shows the average values computed for d_m . The smallest molecule is water, and the largest ones are BL, DBE, and BMF. As seen, in each polymer zone K_0 values decrease as the molecules are bulkier. According to K_0 values, the polymer zone of chain density 0.2 nm/nm³ is accessible to all reactants and reaction

products. In the zone of density 0.4 nm/nm³, fructose, 1-butanol, HMF, LA, and BF have a distribution coefficient relatively high, but the accessibility of the bulkiest molecules (BL, DBE, and BMF) is limited. Finally, the stiffer zones of resins (chain density 0.8 and 1.5 nm/nm³) are moderately accessible to fructose, 1-butanol, LA, BF, and HMF. However, BL, DBE, and BMF are practically excluded. Water penetrates easily into all the polymer zones, even the more impervious, favoring resin swelling. Therefore, the accessibility of the compounds to the different polymer zones of the swollen resin could explain the different activity shown by tested catalysts. Like water, formic acid penetrates easily in all the resin zones.

Table 6. Equivalent pore diameter and Ogston distribution coefficients, K_0 , in the zones of different gel-phase density in swollen resins. The diameter of randomly distributed rigid rods representing polymer chains is $d_c = 0.4$ nm

Polymer chain density (nm/nm ³)	0.1	0.2	0.4	0.8	1.5	
Equivalent pore diameter (nm)	9.3	4.8	2.6	1.5	1.0	
Compound	d_m (nm)		K_0			
Water	0.150	0.98	0.95	0.91	0.83	0.70
Formic acid	0.305	0.96	0.92	0.86	0.73	0.56
HMF	0.602	0.92	0.85	0.73	0.53	0.31
1-Butanol	0.636	0.92	0.84	0.71	0.51	0.28
Levulinic acid	0.679	0.91	0.83	0.69	0.48	0.25
Butyl formate	0.772	0.90	0.81	0.65	0.42	0.20
Fructose	0.772	0.90	0.81	0.65	0.42	0.20
Butyl levulinate	1.006	0.86	0.73	0.54	0.29	0.10
DBE	1.131	0.83	0.69	0.48	0.23	0.06
BMF	1.175	0.82	0.68	0.46	0.21	0.05

Tested resins have a similar acid capacity (Table 1) and acid site strength [31], therefore their different catalytic behavior in 1-butanol/water solution can be attributed mainly to their morphology in a swollen state. As Table 5 and Fig. 7 show, ΣV_{sp} and the spaces that appear when resins swell are very different and give rise to a distinct reaction arena in each catalyst. Dowex 50Wx2 has the highest ΣV_{sp} and the widest spaces open on swelling (polymer density 0.2-0.4 nm/nm³; equivalent to 2.6-4.8 nm pores [66]), whereas Amberlyst 15 has the lowest ΣV_{sp} and the open spaces on swelling are the narrowest (polymer density 1.5 nm/nm³; equivalent to 1-nm pores [66]). Consequently, the volume of liquid inside the Dowex resin is greater than in the Amberlyst 15, and in the latter, the open spaces are much narrower. In the case of Dowex 50Wx2, the molecules of all compounds are considerably smaller than the equivalent pore diameter of gel-phase spaces (4.8-2.6 nm), and the K_0

values ensure that their concentrations in the gel-phase are similar to the bulk environment. In the case of Amberlyst 15, the size of the bulkiest compounds is of the same order as spaces within the gel-phase (1.0 nm) and the low K_0 values suggest that they tend to be excluded from the gel phase. Fructose initially would be present in the gel-phase of Dowex 50Wx2 in concentrations close to the bulk phase, producing readily HMF. Since K_0 for HMF (0.85-073) is high, it tends to remain in the gel phase and reacts producing LA, BMF, and BL according to the reaction scheme. In the case of Amberlyst 15, fructose has a very low value of K_0 (0.20). It can be inferred that although fructose penetrates inside the resin, the amount of the monosaccharide in the gel-phase is lower than in Dowex 50Wx2, and as Fig. 5A shows, it reacts slowly. The distribution coefficient of HMF (0.31) is lower than in the gel-type resin, and HMF tends to go out to the bulk liquid rather than remain in the pores and continue the reaction. The size of LA and BMF is closer to the width of spaces open. The low K_0 values for both LA and BMF suggest that they tend to be excluded from the gel phase, producing a small BL amount. Amberlyst 39 in a swollen state shows a noticeable ΣV_{sp} with a polymer zone of density 0.4 nm/nm³. The production of most of the compounds of the reaction scheme is like that of Dowex 50Wx2, except in the case of BMF. Amberlyst 39 also have an impervious zone of density 1.5 nm/nm³. The very low K_0 value of BMF in this polymer fraction (0.05) may explain the lower BMF yield observed. Therefore, the different yields of Table 3 are related to the morphology of resins swollen in the reaction medium: resins able to highly swell are more effective in producing butyl levulinate.

In water/alcohol media, where resins largely swell by the interaction with the polar liquid, the density of acid sites in the swollen polymer ($[H^+]/\Sigma V_{sp}$, a measure of the mean density of acid sites in the swollen resin) illustrates better the influence of morphology than ΣV_{sp} [31,42,43]. Fig. 8 shows the yield of products and byproducts at 6 and 8 h of reaction. There is an almost linear relationship between the yield of BMF (Fig. 8C) and BL (Fig. 8D) against $[H^+]/\Sigma V_{sp}$ showing that resins with low acid site density perform better to synthesize BMF and BL. The best values are found on Dowex 50Wx2 and Dowex 50Wx4 whereas the worst one was obtained on Amberlyst 15. Correspondingly, HMF yield increases with $[H^+]/\Sigma V_{sp}$ showing that formation and decomposition of HMF require wide spaces in the swollen resins and a low density of acid sites (Fig 8A). BF production is favored in low acid density resins (Fig 8F), whereas that of LA (Fig. 8B) and FA (Fig. 8E) is almost independent on $[H^+]/\Sigma V_{sp}$. It can be hypothesized that HMF formation and conversion to BMF, BF, and BL might probably require the contribution of at least two acid sites [67]. The reaction mechanisms to produce these substances require adequate distances between acid centers which are more easily found in highly swollen resins with a low density of acid sites due to their more flexible morphology.

Therefore, acid site density has a relevant role in this reaction network. Since HMF, BMF, BL, and BF are relatively bulky, swollen resins with lower acid site density perform better. The best catalyst (Dowex 50Wx2) has the maximum ΣV_{sp} value and therefore the lowest $[H^+]/\Sigma V_{sp}$ one. On the contrary, the formation of FA and LA is almost independent on $[H^+]/\Sigma V_{sp}$.

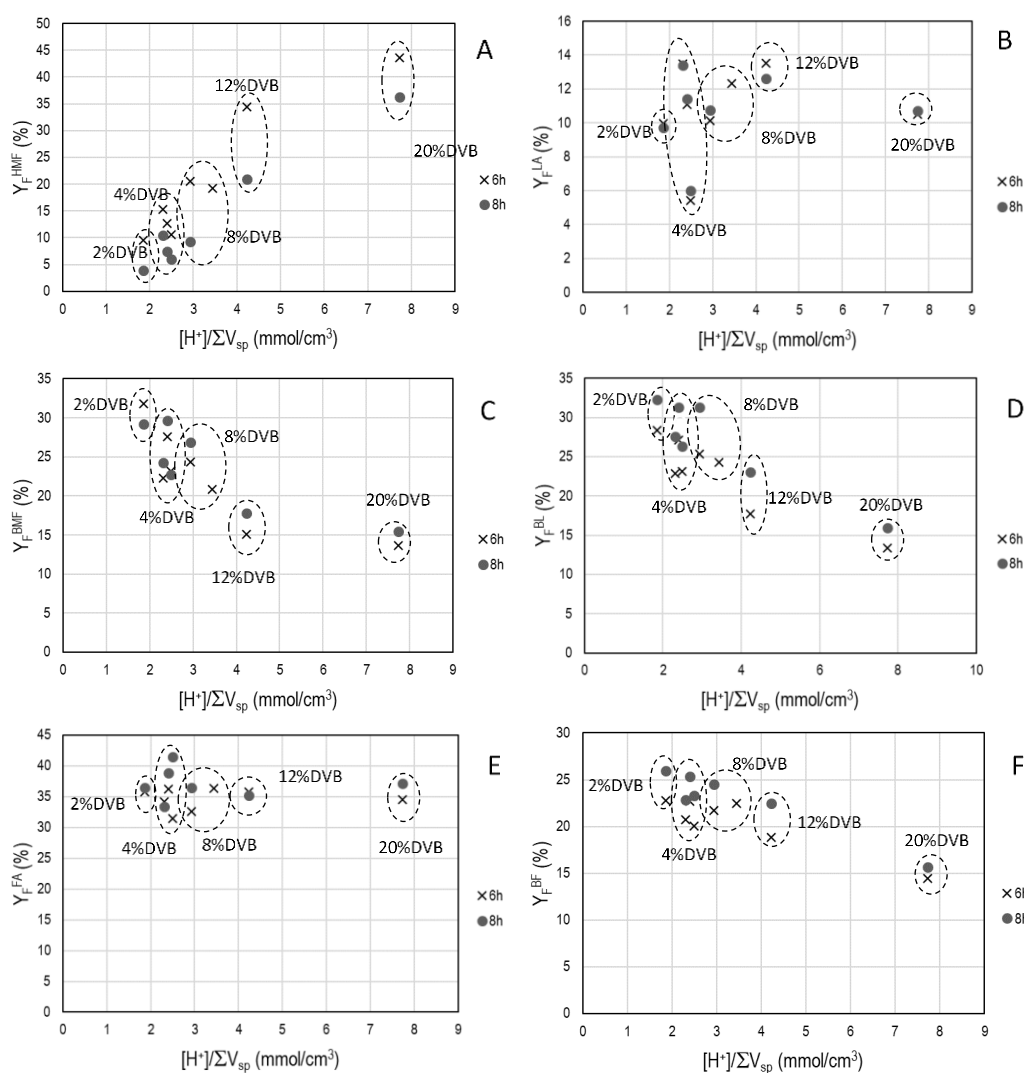


Figure 8. HMF (A), LA (B), BMF (C), BL (D), FA (E), and BF (F) yield as a function of $[H^+]/\Sigma V_{sp}$ at 6 and 8h. $T=120^\circ\text{C}$, $R_{BuOH/F}=79$; $R_{BuOH/W}=1.19$; 1g dried catalyst; catalyst loading 1.7 wt. %.

3.7. Humins formation

The reaction medium is dark brown at the end of the experiments showing the formation of soluble and insoluble polymers, called humins, because of the degradation reactions of fructose [52], HMF

[56], and/or cross-reaction between fructose and HMF [57]. Such compounds are difficult to quantify by analytical methods because of the number of polymers that are formed. Thus the formation of humins may be computed in terms of the decrease in the carbon balance, assuming that all the compounds of the main pathway are identified and all the lack of carbon is due to the formation of these polymers [68]. Both the mole balance of fructose and the carbon atom balance of fructose at 6h are shown in Table 7. In general, fructose loss is 3% higher than fructose carbon atoms, which is consistent with the stoichiometric excess of FA (plus BF) observed in most experiments. It was observed that fructose loss is remarkable in the two first hours of the experiment and then increases slowly with time.

Table 7. Fructose moles and fructose carbon atoms lost forming humins at 6h reaction time ($R_{\text{BuOH/F}} = 79$; $R_{\text{BuOH/W}} = 1.19$)

Entry	Catalyst	Experimental conditions	C atoms lost (%)	Fructose mole lost (%)
1	Dowex 50Wx2	80°C, 1 g, fresh resin	0	0
2	Dowex 50Wx2	90°C, 1 g, fresh resin	0	0
3	Dowex 50Wx2	100°C, 1 g, fresh resin	1,7	3.6
4	Dowex 50Wx2	110°C, 1 g, fresh resin	13.1	16.7
5	Dowex 50Wx2	120°C, 1 g, fresh resin	16.7	20.1
6	Dowex 50Wx2	120°C, 0.5 g, fresh resin	16.6	20.3
7	Dowex 50Wx2	120°C, 2.0 g, fresh resin	12.3	17.0
8	Dowex 50Wx4	120°C, 1 g, fresh resin	18.0	21.4
9	CT 124	120°C, 1 g, fresh resin	33.0	36.9
10	Amberlyst 31	120°C, 1 g, fresh resin	22.5	25.6
11	Dowex 50Wx8	120°C, 1 g, fresh resin	18.9	22.6
12	Amberlyst 39	120°C, 1 g, fresh resin	16.1	19.3
13	Amberlyst 16	120°C, 1 g, fresh resin	14.9	18.8
14	Amberlyst 15	120°C, 1 g, fresh resin	14.7	16.7
15	Dowex 50Wx2	120°C, 1 g, 1 st reuse cycle	19.6	23.1
16	Dowex 50Wx2	120°C, 0.7 g, 2 nd reuse cycle	18.7	22.4

Entries 1 to 5 show that humins formation increases with temperature. On Dowex 50Wx2, fructose loss is negligible at 80 and 90°C: the liquid is only slightly yellow after runs. Some degradation to humins is observed at 100°C (entry 3), and fructose loss increases substantially at 110 and 120°C (entries 4 and 5). On comparing the loss of fructose in the experiments performed at 120°C on different resins (entries 5, 8-14), no clear trend is seen. On the one hand, it seems that humins are formed in higher amounts on the more active resins (Dowex 50Wx2 and Dowex 50Wx4). As in the

less active resins (Amberlyst 16 and Amberlyst 15), the amount of HMF is still high at 6h (Fig. 5B, Table 3), this fact could highlight the contribution of HMF to the formation of humins. However, the highest values observed on Amberlyst 31 and, particularly, CT124 that have the same DVB% and a similar morphology in the swollen state as Dowex 50Wx4 (Fig. 7, Table 5), suggest that humins formation is a very complex process deserving a specific study. On the other hand, experiments with a different mass of Dowex 50Wx2 (entries 5-7) show that the formation of humins decreases slightly on increasing catalyst mass. This fact could indicate that homogeneous reactions play a role in the degradation of fructose and HMF to humins, and the formation of HMF, BMF, LA, and BL accelerates by using larger catalyst mass limiting in this way the extent of catalytic degradation reactions of fructose and HMF.

3.8. Catalyst reusability

Experiments with reused Dowex 50Wx2 were performed at 120°C. After each run, resin samples were washed and dried by the procedure described in section 2.5. Results with fresh and reused catalysts are shown as a function of contact time since in the second reusing cycle the experiment was performed with a catalyst mass significantly lower. As seen in Fig. 9A, fructose readily reacts on reused resin and the conversion of fructose is almost complete at a contact time higher than 400 h·g/mol of fructose. Interestingly, reused catalyst gives rise to lower BL and BMF formation, but higher HMF formation. HMF forms and decomposes on reused resin at a lower reaction rate and the yield curves are above that of fresh resin (Fig. 9B). It is also seen that the maximum yield of HMF on reused resin appears at a longer contact time. As for BL, the yield is about 25% lower over reused resin, although the curves for first and second reuse overlap (Fig. 9E). The yields of BMF (Fig. 9D) and BF (not shown) in the second reuse are intermediate between those of fresh and first reuse cycles. The yield of LA on the fresh and reused catalyst are similar within the limits of the experimental error, although values on the reused resin are a bit higher (Fig. 9C). Formation of FA over the reused resin (not shown) is slower at the beginning of the reaction, but at long reaction time, FA yield over fresh and reused catalyst tends to the same value within the limits of the experimental error. Although more cycles with reused catalysts are necessary to evaluate the catalyst span, it is a promising fact that runs carried out with reused resin give similar results. Finally, humins formation on fresh and reused resins is also of the same order (Table 7, entries 5, 15, and 16).

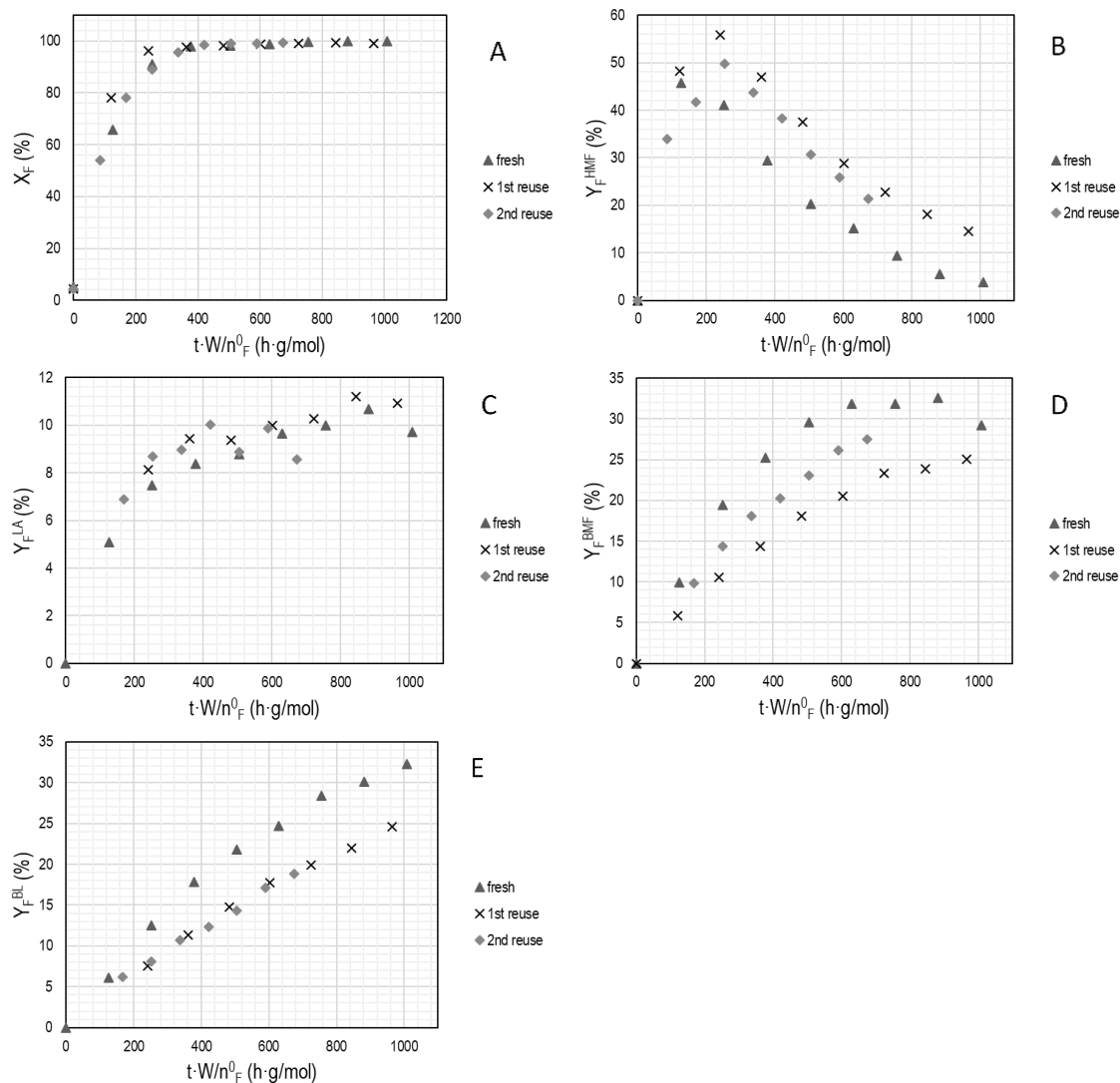


FIG. 9. Fructose conversion (A) and HMF (B), LA (C), BMF (D), and BL (E) yield over fresh and reused Dowex 50Wx2 against contact time on a catalyst mass basis. $T = 120^\circ\text{C}$; $R_{\text{BuOH}/F} = 79$; $R_{\text{BuOH}/W} = 1.19$; fresh and first reuse cycle: 1g dried resin (catalyst loading 1.7 wt. %); second cycle: 0.7 g dried resin (catalyst loading 1.2 wt. %)

The behavior of reused catalysts might be due to both the loss of active sites and the formation of polymers (solid humins) covering the resin during the reaction. To ascertain the cause of such behavior, fresh and reused Dowex 50Wx2 were titrated against standard base after each run, and S distribution was studied with SEM/EDS. As Table 8 shows, after the second reuse cycle, the acid capacity of resin as determined by titration decreases 47% compared to fresh resin. EDS analyses show that the percentage of S atoms decreases on reusing the resin, whereas that of O atoms increases. The percentage of C atoms decreases only slightly. Since the loss of S atoms after the

second reuse cycle as determined by EDS is only of 25% compared to the fresh catalyst, it can be inferred that in addition to deactivation for loss of sulfonic groups, the reaction rate is limited by organic polymers covering the resin and thus several sulfonic groups. The presence of polymers agrees with the fact that the percentage of O atoms in the reused catalyst increases, as measured by EDS since humins covering the resin consist of a furan-rich polymer network containing different oxygen functional groups [56]. Therefore, both desulfonation and fouling by humins might explain the loss of activity on a catalyst mass basis observed.

Table 8. SEM/EDS analysis and acid capacity of fresh and reused Dowex 50Wx2

Catalyst	[H+] (mmol/g) ^a	EDX analysis		
		% C atoms	% O atoms	% S atoms
Fresh resin	4.98	74.54	15.78	8.68
Fresh resin, after use	4.13	74.69	17.45	7.56
After 1 st reuse cycle	3.35	72.74	20.02	7.25
After 2 nd reuse cycle	2.65	73.24	20.34	6.37

^a Titration against standard base by the Fischer and Kunin method [45]

If data of the reused resin are plotted against contact time on an acid site basis, activity per acid site as determined by titration (Table 8) of fresh and reused resin is very similar, in particular in the second reuse cycle (Fig. 10). This fact suggests that humins block predominantly acid sites located in the most impervious resin zones. Such acid sites hardly take part in the reaction since such zones are almost inaccessible to reactants, even in a swollen state. Sulfonic groups blocked by humins cannot be measured by titration because humins prevent the reaction with the base. It confirms that BL production occurs in the swollen gel-phase of the resin, wide and flexible enough for the reactions of the series-parallel scheme (Figure 2) to take place.

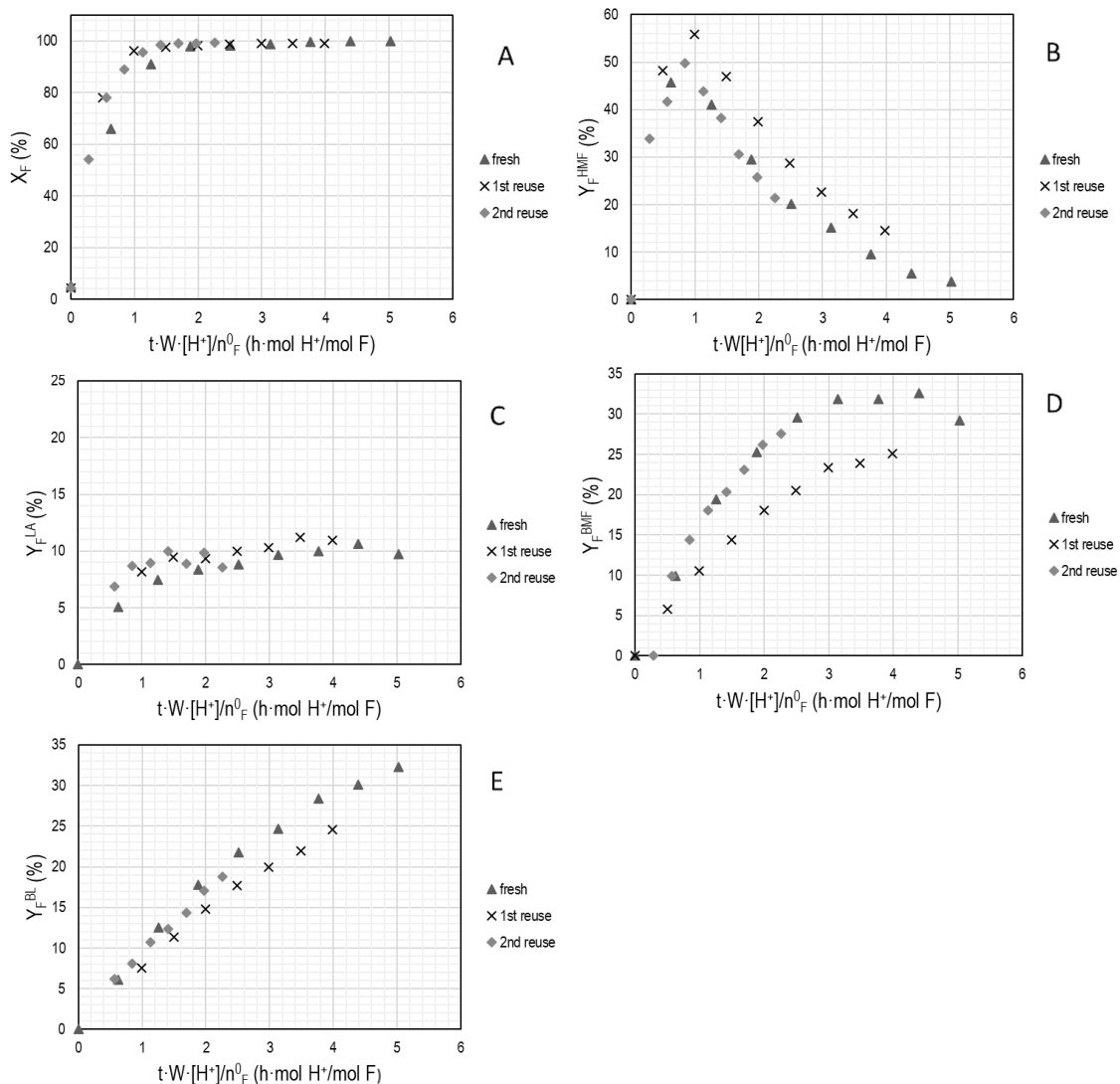


FIG.10. Fructose conversion (A) and HMF (B), LA (C), BMD (D), and BL (E) yield over fresh and reused Dowex 50Wx2 against contact time on an acid site basis. $T = 120^\circ\text{C}$; $R_{\text{BuOH}/F} = 79$; $R_{\text{BuOH}/W} = 1.24$; fresh and first reused resin: 1g dry resin (catalyst loading 1.7 wt. %); second reuse: 0.7 g dried resin (catalyst loading 1.2 wt. %)

3.9. Comparison with literature data

Data of the BL synthesis from fructose found in the open literature on solid catalysts are compared in Table 9 with the best ones obtained in the present work. The comparison is not straightforward since different reaction conditions and devices are used in the open literature. For easy comparison, the reaction conditions are shown through parameters as initial molar ratio 1-butanol/fructose, etc. As seen, in all these works 1-butanol free of water is used in large excess compared to fructose. In this way, the system shifts to BL production, and, at the same time, humins formation is reduced [57,69].

It is to be noted that the information supplied is generally limited, and important details of the course of reactions are not given i.e. humins formation, the FA (plus BF) excess over LA (plus BL), or the yield of products other than BL. Only some of these papers report the yield of BMF produced.

As Table 8 shows, the best BL yield obtained with Dowex 50Wx2 (entry 1) is lower than the yields found in the literature. This is probably due to the presence of water initially since water highly inhibits the catalytic activity of ion exchange resins in alcohol media [44,70-72]. An additional experiment on Dowex 50Wx2 was performed with water-free 1-butanol (entry 2). As seen, BL yield highly increases, and it is of the same order as those found in the open literature. It is to be noted that some BMF is in the reaction medium at 8h and therefore BL yield could still increase with time. Regarding the experiment carried out with a 1-butanol/water mixture (entry 1), it is also noticeable the decrease in humins production that is consistent with the reduction of the stoichiometric excess of FA (plus BF) observed (1.29 vs. 1.45).

Experiments performed over Amberlyst 15 and CNT-PSSA at 120°C (entry 5) show BL yields higher than entry 2 although a higher excess of 1-butanol is used. Brown et al. [73] reported on Amberlyst 15 at 100°C (entry 3) a similar BL yield as that found by us with water-free 1-butanol (entry 2). However, Balakrishnan et al. reported at 110°C very low BL yields on Amberlyst 15 and Dowex 50Wx8 (entry 4) [40]. In line with our experiments, a large amount of BMF remains in the reactor yet what suggests that a higher BL amount could be obtained at longer contact times. However, in the last two works, very large catalyst loading, and contact time were used and such excessive catalyst loading might likely cause saturation problems by solids inside the reactor.

As for inorganic catalysts (entries 6 and 7), runs were performed at a higher temperature and a faster reaction is expected. However, BL yield on TiO₂ (entry 6) is lower than that reported with Dowex 50Wx2 in entry 2. The formation of humins on TiO₂ (not reported) may be important enough to decrease BL formation since inorganic catalysts show deactivation after a few cycles.

In summary, the use of ion-exchange resins, particularly those highly swollen in aqueous-alcoholic media, is interesting because good BL yields can be obtained at a moderate temperature. Energy savings could be significant in industrial practice so that the production of BL from fructose is a greener process

Table 9. Comparison with literature data on the transformation of fructose to butyl levulinate

Entry	Catalyst	T(°C)	Reaction conditions	Reaction Parameters ^a	t(h)	Wt/n _F ⁰ g·h/mol	X _F (%)	Y _F ^{BL} (%)	Y _F ^{BMF} (%)	Observation	Ref
1	Dowex 50Wx2	120	Catalyst: 2 g Fructose: 1.5 g BuOH: 60 mL Water: 10 mL	R _{BuOH/F} = 79 R _{BuOH/W} = 1.19 m _F /W = 0,75 Cat. Load. = 3.3%	8	1920	>99	43.4	25.1	Humins: 17.0% FA excess: 1.45 Reuse: Y _F ^{BL} decreases by 22% after 3 cycles	This work
2	Dowex 50Wx2	120	Catalyst: 1 g Fructose: 1.8 g BuOH: 70 mL Water: 0 mL	R _{BuOH/F} = 79 m _F /W = 1.8 Cat. Load. = 1.7%	8	800	100	73.4	10.4	Humins: 9.8% FA excess: 1.29	This work
3	Amberlyts 15	100	Catalyst: 20 g Fructose: 20 g BuOH: 150 mL Water: 0 mL	R _{BuOH/F} = 14.7 m _F /W = 1 Cat. Load. =12.4%	20	3600	na	77	0		[73]
4	Amberlyst 15	110	Catalyst 0.65 g Fructose: 0.18 g BuOH: 2g Water: 0 mL	R _{BuOH/F} = 270 m _F /W = 0.28 Cat. Load. = 23%	30	1950	97	16	71		[40]
	Dowex 50Wx8						97	14	56		
5	Amberlyst 15	120	Catalyst 20 mg Fructose: 50 mg BuOH: 4 mL Water: 0 mL	R _{BuOH/F} = 156 m _F /W = 2.5 Cat. Load. = 0.6%	24	2160	>99	89		Reuse: Y _F ^{BL} decreases by 18% after 6 cycles	[41]
	CNT-PSSA						>99	87			
6	TiO ₂ nanoparticles	150	Catalyst 0.2 g Fructose: 0.8 g BuOH: 40 mL Water: 0 mL	R _{BuOH/F} = 98 m _F /W = 4 Cat. Load. = 4.8%	3	135	100	62.8			[39]
7	Fe ₂ (SO ₄) ₃	190	Catalyst 0.1 g Fructose: 0.18 g BuOH: 20 mL Water: 0 mL	R _{BuOH/F} = 217 m _F /W = 1.8 Cat. Load. = 0.6%	3	300	>99	75		Reuse: Y _F ^{BL} decreases by 27% after 5 cycles	[37]

^a m_F/W = quotient of fructose to catalyst mass; Cat. Load. = Catalyst loading

^b FA excess = quotient between the sum of FA and BF moles produced and the sum of BL and LA

4. Conclusions

Ion exchange resins are effective catalysts to produce butyl levulinate from fructose. BL formation has been studied in the temperature range 80-120°C at 2.0 MPa in the liquid phase using a BuOH/water mixture ($R_{\text{BuOH/W}} = 1.19$). The process is highly temperature-sensitive, and BL production is detected only above 100°C. Butyl levulinate formation follows two pathways. Firstly, fructose dehydrates to HMF, which in turn reacts with water or 1-butanol. HMF hydrolysis gives rise to LA and FA, and the etherification of HMF yields BMF. Finally, esterification of LA with butanol and alcoholysis of BMF yield butyl levulinate. BL synthesis is highly influenced by the morphology of the acidic ion-exchange resins in the liquid reaction medium. Acidic resins greatly swell in butanol-water mixtures, and the quality of spaces formed in the swollen polymer network is decisive. Resins showing the best catalytic behavior are those that highly swell in the reaction medium and have less acid site density in the swollen state. In this way, gel-type Dowex 50Wx2 (2% DVB) is the most effective resin in terms of BL yield. The formation of butyl levulinate is accompanied by the formation of humins due to the degradation of fructose, HMF, and fructose-HMF cross-reaction. The mole balance of fructose and the carbon atom balance of fructose show that between 17 and 37% of monosaccharide is lost forming humins. Finally, experiments with reused resin show that the activity of fresh and twice-reused catalysts is similar on an acid site basis. The loss of activity on a resin weight basis can be explained by desulfonation and fouling because of humins deposition over the most impervious polymer zone. The acid centers of such impervious polymer zone hardly take part in the reaction, so the activity per accessible site does not change.

Credit Author statement

Eliana Ramírez: investigation, methodology. **Roger Bringué:** visualization, writing – review & editing. **Carles Fité:** Validation, formal analysis. **Montserrat Iborra:** Investigation, resources, methodology. **Javier Tejero:** Supervision, writing - original draft, conceptualization, project administration. **Fidel Cunill:** Conceptualization, writing – review & editing

Declaration of interest:

The authors declare that they have no competing financial interests or personal relationships that could have appeared to influence the work reported in this paper

Funding

Grant CTQ2014-56618-R from the Spanish Ministry of Economy and Competitiveness is kindly acknowledged.

Acknowledgments

We thank Rohm and Haas France for supplying Amberlyst resins, and Purolite for supplying CT resin.

Nomenclature

Als	Alkyl levulinates
a_m	External surface area per unit mass of catalyst (m^2/g)
BF	Butyl formate
BL	Butyl levulinate
BMF	5-Butoxymethylfurfural
BuOH	1-Butanol
C	Polymer chain density in the swollen state, nm/nm^3 .
$C_{F,b}$	Fructose concentration in the bulk liquid, mol/L
$C_{F,S}$	Fructose concentration in the external catalyst surface, mol/L
DBE	Di-n-butyl ether
$D_{e,F}$	Fructose effective diffusivity in the resin particle, m^2/h
d_c	diameter of polymer chains, nm
d_m	molecule diameter assumed spherical, nm
\bar{d}_p	Mean particle diameter of swelling particle, m
d_{oore}	mean pore diameter, nm
F	Fructose
FA	Formic acid
HMF	5-Hidroxymethylfurfural
K_0	Ogston distribution coefficient
$k_{m,F}$	Mass-transfer coefficient of fructose between the bulk liquid and the resin surface, m/h
L_e	Effective diffusion-path-length parameter, m
LA	levulinic acid

m_F	fructose mass, g
PS-DVB	Polystyrene-divinylbenzene
$R_{BuOH/W}$	Initial mole ratio alcohol/water
$R_{BuOH/F}$	Initial mole ratio 1-butanol/fructose
r_F^0	Initial reaction rate of fructose consumption, mol/h·g
S_g	BET Surface area, m ² /g dry catalyst
S_{pore}	Surface area of resin in the swollen state, m ² /g dry catalyst
t	time, h
V_g	pore volume by N ₂ adsorption-desorption at 77K, cm ³ /g dry catalyst
V_{pore}	Pore volume of resin in the swollen state, cm ³ /g dry catalyst
V_{sp}	Specific volume of the swollen polymer, cm ³ /g dry catalyst
W	mass of dry catalyst, g
X_F	Fructose conversion, dimensionless
Y_F^j	Yield of fructose towards the compound j, dimensionless
θ	Porosity of the swelling catalyst, dimensionless
ρ_P	Apparent density of the catalyst, kg/m ³ .
ρ_S	Skeletal density of the catalyst, kg/m ³ .
Φ	Weisz-Prater Modulus, dimensionless

Literature

1. T. Werpy, G. Petersen, Top Value Added Chemicals from Biomass. Volume I – Results of Screening for Potential Candidates from Sugars and Synthesis Gas. U.S. Department of Energy. DOE/GO-102004-1992, 2004. <http://dx.doi.org/10.2172/15008859>.
2. J.J. Bozell, G.R. Petersen, Green. Chem. 12 (2010) 539-554. <http://dx.doi.org/10.1039/b922014c>
3. J.J. Bozell, L. Moens, D.C. Elliott, Y. Wang, G.G. Neuenschwander, S.W. Fitzpatrick, R.J. Bilski, J.L. Jarnefeld, Resour. Conserv. Recycl. 28 (2000) 227-239. [http://dx.doi.org/10.1016/S0921-3449\(99\)00047-6](http://dx.doi.org/10.1016/S0921-3449(99)00047-6)

4. A. Demirbas, Appl. Energy, 88 (2011) 17-28.
<http://dx.doi.org/10.1016/j.apenergy.2010.07.016>
5. F.X. Covers, Solvent refining oil, U.S. Patent 2087473 (1937)
6. P.D. Bloom, Levulinic acid ester derivatives as reactive plasticizers and coalescent solvents U.S. Patent 2010/0216915 A1 (2010)
7. J.R. Rieth, C.M. Leibig, J.D. Pratt, M. Jackson, U.S. Latex coating compositions including carboxy ester ketal coalescents, methods of manufacture and uses thereof. U.S. Patent Application 2012/0041110 A1 (2012)
8. D.J. Yontz, Fragrant formulations, methods of manufacture thereof and articles comprising the same, U.S. Patent 2011/0274643 A1 (2011)
9. L. Lomba, B. Giner, I. Bandrés, C. Lafuente, M.R. Pino, Green Chem. 13 (2011) 2062-2070.
<http://dx.doi.org/10.1039/c0gc00873b>
10. H.G. Pöttering, P. Necas. Off. J. Eur. Union. 140 (2009) 88-112
11. J. Yanowitz, E. Christensen, R.L. McCormick. Utilization of renewable oxygenates as gasoline blending components. Technical report NREL/TP-5400-50791. 2011
12. E. Christensen, J. Yanowitz, M. Ratcliff, R.L. McCormick, Energy Fuels, 25 (2011) 4723-4733.
<http://dx.doi.org/10.1021/ef2010089>
13. H. Joshi, B.R. Moser, J. Toler, W.F. Smith, T. Walker, Biomass Bioenergy 35 (2011) 3262-3266.
<http://dx.doi.org/10.1016/j.biombioe.2011.04.020>
14. R.W. Jenkins, M. Munro, S. Nash, C.J. Chuck, Fuel 103 (2013) 593-599.
<http://dx.doi.org/10.1016/j.fuel.2012.08.019>
15. A. Demolis, N Essayem, F. Rataboul, ACS Sustain. Chem. Eng. 2 (2014) 1338-1352.
<http://dx.doi.org/10.1021/sc500082n>.
16. P.P.T. Sah, S.Y. Ma, J. Am. Chem. Soc. 52 (1930) 4880-4883.
<http://dx.doi.org/10.1021/ja01375a033>
17. H.A. Schuette, M.A. Cowley, J. Am. Chem. Soc. 53 (1931) 3485-3489.
<http://dx.doi.org/10.1021/ja01360a039>
18. G.J. Cox, M.L. Dodds, J. Am. Chem. Soc. 55 (1933) 3391-3394.
<http://dx.doi.org/10.1021/ja01335a59>
19. H.J. Bart, J. Reidetschmeger, K. Schatka, A. Lehmann, Ind. Eng. Chem. Res. 33 (1994) 21-25.
<http://dx.doi.org/10.1021/ie00025a004>
20. K.C. Maheria, J. Kozinsji, A. Dalai, Catal. Lett. 143 (2013) 1220-1225.
<http://dx.doi.org/10.1007/s10562-013-1041-3>.
21. K.Y. Nandiwale, V.V. Bokade, Chem. Eng. Technol. 38 (2015) 246-252.
<http://dx.doi.org/10.1002/ceat.201400326>.
22. F.G. Cirujano, A. Corma, F.X. Llabrés, Chem. Eng. Sci. 124 (2015) 52-60.
<http://dx.doi.org/10.1016/j.ces.2014.09.047>.
23. S. Dharme, V.V. Bokade, J. Nat. Gas Chem. 20 (2011) 18-24.
[http://dx.doi.org/10.1016/S1003-9953\(10\)60147-8](http://dx.doi.org/10.1016/S1003-9953(10)60147-8).
24. K. Manikandan, K.K. Cheralathan, Appl. Catal. A: Gen. 547 (2017) 237-247.
<http://dx.doi.org/10.1016/j.apcata.2017.09.007>.
25. M. Popova, A. Szegedi, H. Lazarova, A. Ristic, Y. Kalvachev, G. Atanasova, N. Wilde, N. Novak Tusar, R. Glaser, Micro. Meso. Mat. 235 (2016) 50-58.
<http://dx.doi.org/10.1016/j.micromeso.2016.07.047>.
26. F. Su, Q. Wu, D. Song, X. Zhang, M. Wang, Y. Guo, J. Mat. Chem. A 1 (2013) 13209-13221.
<http://dx.doi.org/10.1039/c3ta12412f>.

27. D. Song, S. An, Y. Sun, Y. Guo. *J. Catal.* 333 (2016) 184-199.
<http://dx.doi.org/10.1016/j.jcat.2015.10.018>.
28. W. Ciptonugroho, M.G. Al-Shaal, J.B. Mensah, R. Palkovits, *J. Catal.* 340 (2016) 17-29.
<http://dx.doi.org/10.1016/j.jcat.2016.05.001>.
29. X. Zhou, Z. Xain Li, C. Zhang, X. Ping Gao, Y. Zhi Dai, G. Ying Wang, *J. Mol. Catal. A: Chem.* 417 (2016) 71-75. <http://dx.doi.org/10.1016/j.nolcata.2016.03.006>.
30. A.N. Chermahini, M. Nazeri, *Fuel. Proc. Technol.* 167 (2017) 442-450.
<http://dx.doi.org/10.1016/j.fuproc.2017.07.034>.
31. M.A. Tejero, E. Ramírez, C. Fité, J. Tejero, F. Cunill. *Appl. Catal. A: Gen.* 517 (2016) 56-66.
<http://dx.doi.org/10.1016/j.apcata.2016.02.032>.
32. V. Trombettoni, L. Bianchi, A. Zupanich, A. Porciello, M. Cuomo, O. Piermatti, A. Marrochi, L. Vaccaro, *Catalysts* 7 (2017) 235. <http://dx.doi.org/10.3390/catal7080235>.
33. G.D. Yadav, I.V. Borkar, *Ind. Eng. Chem. Res.* 47 (2008) 3358-3363.
<http://dx.doi.org/10.1021/ie800193f>.
34. Y. Hishikawa, M. Yamaguchi, S. Kubo, Y. Yamada, *J. Wood Sci.* 59 (2013) 179-182.
<http://dx.doi.org/10.1007/s10086-013-1324-8>.
35. A. Demolis, M. Eternot, N. Essayem, F. Rataboul, *New J. Chem* 40 (2016) 3747-3754.
<http://dx.doi.org/10.1039/c5nj02493e>.
36. F. Yu, R. Zhong, H. Chong, M. Smet, W. Dehaen, B.F. Sels, *Green Chem.* 19 (2017) 153-163.
<http://dx.doi.org/10.1039/c6gc02130a>.
37. R. An, G. Xu, Ch. Chang, J. Bai, S. Fang, *J. Energy Chem.* 26 (2017) 556-563.
<http://dx.doi.org/10.1016/j.jechem.2016.11.015>.
38. L. Deng, Ch. Chang, R. An, X. Qi, G. Xu, *Cellulose* 24 (2017) 5403-5415.
<http://dx.doi.org/10.1007/s10570-017-1530-4>.
39. C.H. Kuo, A.S. Poyraz, L. Jin, Y. Meng, L. Pahalagedara, S.Y. Chen, D.A. Kriz, C. Guild, A. Gudz, S.L. Suib, *Green Chem.* 16 (2014) 785-791. <http://dx.doi.org/10.1039/c3gc40909k>
40. M. Balakrishnan, E.R. Sacia, A.T. Bell, *Green Chem.* 14 (2012) 1626-1634.
<http://dx.doi.org/10.1039/c2gc35102a>.
41. R. Liu, J. Chen, X. Huang, L. Chen, L. Ma, X. Li, *Green Chem.* 15 (2013) 2895-2903.
<http://dx.doi.org/10.1039/c3gc41139g>.
42. R. Bringué, E. Ramírez, M. Iborra, J. Tejero, F. Cunill, *J. Catal.* 304 (2013) 7-21.
<http://dx.doi.org/10.1016/j.jcat.2013.03.006>
43. C. Casas, R. Bringué, E. Ramírez, M. Iborra, J. Tejero, *Appl. Catal. A: Gen.* 396 (2011) 129-139.
<http://dx.doi.org/10.1016/j.apcat.2011.02.006>
44. M.A. Pérez, R. Bringué, M. Iborra, J. Tejero, F. Cunill. *Appl. Catal. A: Gen.* 482 (2014) 38-48.
<http://dx.doi.org/10.1016/j.apcata.2014.05.017>
45. S. Fischer, R. Kunin, *Anal. Chem.* 27 (1955) 1191-1194.
<http://dx.doi.org/10.1021/ac60103a052>
46. R. Soto, M. Svärd, V. Verma, L. Pradela, K. Ryan, A.C. Rasmuson. *Int. J. Pharma.* 588 (2020) 119686. <http://dx.doi.org/10.1016/j.ijpharm.2020.119686>.
47. R. Stephenson, J. Stuart. *J. Chem. Eng. Data* 31 (1986) 56-70.
<http://dx.doi.org/10.1021/je00043a19>.
48. L.A. Reber, W.M. McNabb, W.W- Lucasse. *J. Phys. Chem* 46 (1942) 500-511.
<http://dx.doi.org/10.1021/j150418a010>.
49. N. Ebrahimi, R. Sadeghi, B.A.H. Ameen. *J. Mol. Liquids* 278 (2019) 164-174.
<http://dx.doi.org/10.1016/j.molliq.2019.01.011>.

50. I. Thapa, B. Mullen, A. Saleem, C. Leibig, R.T. Baker, J.B. Giorgi, *Appl. Catal. A: Gen.* 539 (2017) 70-79. <http://dx.doi.org/10.1016/j.apcata.2017.03.016>.
51. E. Ahmad, M.I. Alam, K.K. Pant, M.A. Haider. *Green Chem.* 18 (2016) 4804-4823. <http://dx.doi.org/10.1039/c6gc01523a>.
52. T. Flannelly, M. Lopes, L. Kupianen, S. Dooley, J.J. Leahy, *RSC Advances* 6 (2016) 5797-5804. <http://doi.org/10.1039/c5ra25172a>.
53. T.D. Swift, C. Bagia, V. Choudhary, G. Peklaris, V. Nikolakis, D.V. Vlachos, *ACS Catal.* 4 (2014) 259-267. <http://dx.doi.org/10.1021/cs4009495>.
54. L. Deng, J. Li, D.M. Lai, Y. Fu, Q.X. Guo, *Angew. Chem. Int. Ed.* 48 (2009) 6529-6532. <http://dx.doi.org/10.1002/anie.200902281>.
55. W. Zeng, D.G. Cheng, H. Zhang, F. Chen, Xiaoli, Zhan, *Reac. Kinet. Mech. Cat.* 100 (2010) 377-384. <http://dx.doi.org/10.1007/s11144-010-0187-x>.
56. G. Tsilomelekis, M.J. Orella, Z. Lin, Z. Cheng, W. Zheng, V. Nikolakis, D.G. Vlachos, *Green Chem.* 18 (2016) 1983-1993. <http://doi.org/10.1039/c5gc01938a>.
57. X. Hu, C. Lievens, A. Larcher, C.Z. Li, *Bioresour. Technol.* 102 (2011) 10104-10113. <http://dx.doi.org/10.1016/j.biortecg.2011.08.040>
58. J. M. Smith, *Chemical Engineering Kinetics*. 3rd Edition. McGraw-Hill Kogakusha. Aukland. 1981. Pages 389-412.
59. G.B. Froment, K.B. Bischoff. *Chemical Reactor Analysis and Design*. Second Edition. Wiley. New York. 1990. 2a) Pages 125-128. 2b) Page168.
60. Y. Sano, N. Yamaguchi, T. Adachi, *J. Chem. Eng. Jpn.* 7(4) (1974) 255-261
61. B.E. Poling, J.M. Prausnitz, J.P. O'Connell. *The properties of gases and liquids* Fifth Edition. McGraw-Hill. New York. 2001. Pages 11.41 – 11.42
62. K. Jerabek, *ACS Symp. Ser.* 635 (1996) 211-224
63. K. Jerabek, *Anal. Chem.* 57 (1985) 1595-1597. <http://dx.doi.org/10.1021/ac00285a022>
64. K. Jerabek, *Anal. Chem.* 57 (1985) 1598-1602. <http://dx.doi.org/10.1021/ac00285a023>
65. G. Ogston. *Trans. Faraday Soc.* 54 (1958) 1754-1757. <http://dx.doi.org/10.1039/TF958540174>
66. K. Jerabek, L. Holub, in *13th International IUPAC Conference on Polymers and Organic Chemistry*, Montreal, 2009
67. D.R. Fernandes, A.S. Rocha, E.F. Mai, C.J.A. Mota, V. Teixeira da Silva, *Appl. Catal. A: Gen.* 425-426 (2012) 199-204. <http://dx.doi.org/j.apcata.2012.03.020>
68. G. Garces, L. Faba, E. Diaz, S. Ordóñez, *ChemSusChem* 12 (2019) 1-12. <http://dx.doi.org/10.1002/cssc.201802315>
69. X. Hu, S. Kadarwati, S. Wang, Y. Song, M.D. Mahmudul Hasan, Ch. Li, *Fuel. Proc. Technol.* 137 (2015) 212-219. <http://doi.org/10.1016/j.fuproc.2015.04.024>.
70. R. Bingué, E. Ramírez, M. Iborra, J. Tejero, F. Cunill, *Chem. Eng. J.* 246 (2014) 71-78. <http://dx.doi.org/10.1016/j.cej.2014.02.042>.
71. C. Casas, E. Ramírez, C. Fité, M. Iborra, J. Tejero, *AIChE J.* 63 (2017) 3966-3978. <http://dx.doi.org/10.1002/aic.15741>
72. R. Bingué, J. Tejero, M. Iborra, J.F. Izquierdo, C. Fité, F. Cunill, *Top. Catal.* 45 (2007) 181-186. <http://dx.doi.org/10.1007/s11244-007-0262-3>.
73. D.W. Brown, A.J. Floyd, R.G. Kinsman, Y. Roshan-Ali, *J. Chem. Tech. Biotechnol.* 32 (1982) 920-924. <https://dx.doi.org/10.1002/jctb.5030320730>

FIGURE CAPTIONS

Figure 1. Moles of fructose, MF, BMF, LA, BL, FA, and BF over time on Dowex 50Wx2 ($T = 120^{\circ}\text{C}$; $R_{\text{BuOH}/\text{F}} = 79$; $R_{\text{BuOH}/\text{W}} = 1.19$; 1g dried catalyst; catalyst loading 1.7 wt. %)

Figure 2. Reaction scheme [15,49]

Figure 3. Fructose conversion (A) and yield of HMF (B), LA (C), BMF (D), and BL (E) over contact time as a function of catalyst mass (Dowex 50Wx2; $T = 120^{\circ}\text{C}$; $R_{\text{BuOH}/\text{F}} = 79$; $R_{\text{BuOH}/\text{W}} = 1.19$).

Figure 4. Fructose conversion (A) and yield of HMF (B), LA (C), BMF (D), and BL (E) over time as a function of temperature (Dowex 50Wx2; $R_{\text{BuOH}/\text{F}} = 79$; $R_{\text{BuOH}/\text{W}} = 1.19$; 1g dried catalyst; catalyst loading 1.7 wt. %)

Figure 5. Fructose conversion (A) and yield of HMF (B), LA (C), BMF (D), BL (E), FA (F), and BF (G) vs. time on DOW2, A39, and A15 ($T = 120^{\circ}\text{C}$, $R_{\text{BuOH}/\text{F}} = 79$; $R_{\text{BuOH}/\text{W}} = 1.19$; 1g dried catalyst; catalyst loading 1.7 wt. %)

Figure 6. Morphological changes of a gel-type and a macroreticular resin particle during swelling in polar media

Figure 7. Distribution of zones of different polymer density of swollen PS-DVB catalysts determined from ISEC data analysis in aqueous solution

Figure 8. HMF (A), LA (B), BMF (C), BL (D), FA (E), and BF (F) yield as a function of $[\text{H}^+]/\Sigma V_{\text{sp}}$ at 6 and 8h. $T=120^{\circ}\text{C}$, $R_{\text{BuOH}/\text{F}} = 79$; $R_{\text{BuOH}/\text{W}} = 1.19$; 1g dried catalyst; catalyst loading 1.7 wt. %.

Figure 9. Fructose conversion (A) and HMF (B), LA (C), BMF (D), and BL (E) yield over fresh and reused Dowex 50Wx2 against contact time on a catalyst mass basis. $T= 120^{\circ}\text{C}$; $R_{\text{BuOH}/\text{F}} = 79$; $R_{\text{BuOH}/\text{W}} = 1.19$; fresh and first reuse cycle: 1g dried resin (catalyst loading 1.7 wt. %); second cycle: 0.7 g dried resin (catalyst loading 1.2 wt. %)

Figure 10. Fructose conversion (A) and HMF (B), LA (C), BMD (D), and BL (E) yield over fresh and reused Dowex 50Wx2 against contact time on acid sites basis. $T= 120^{\circ}\text{C}$; $R_{\text{BuOH}/\text{F}} = 79$; $R_{\text{BuOH}/\text{W}} = 1.19$; fresh and first reused cycle: 1g dried resin (catalyst loading 1.7 wt. %); second cycle: 0.7 g dried resin (catalyst loading 1.2 wt. %)